Title

OCT-Detected Optic Nerve Head Neural Canal Direction, Obliqueness, and Minimum Cross-Sectional Area in Healthy Eyes

Authors

Hong, Seungwoo
Yang, Hongli
Gardiner, Stuart K
et al.

Publication Date

2019-12-01

DOI

10.1016/j.ajo.2019.05.009

Peer reviewed

HHS Public Access

Author manuscript

Am J Ophthalmol. Author manuscript; available in PMC 2020 December 01.

Published in final edited form as:

Am J Ophthalmol. 2019 December ; 208: 185–205. doi:10.1016/j.ajo.2019.05.009.

OCT-Detected Optic Nerve Head Neural Canal Direction, Obliqueness and Minimum Cross-Sectional Area in Healthy Eyes

Seungwoo Hong, MD, PhD[1,2], **Hongli Yang, PhD**[1], **Stuart K Gardiner, PhD**[3], **Haomin Luo, MD**[1,4], **Christy Hardin, MA**[1], **Glen P. Sharpe, MSc**[5], **Joseph Caprioli, MD**[6], **Shaban Demirel, OD, PhD**[3], **Christopher A. Girkin, MD, MSPH**[7], **Jeffrey M. Liebmann, MD**[8], **Christian Y. Mardin, MD**[9], **Harry A. Quigley, MD**[10], **Alexander F. Scheuerle, MD**[11], **Brad Fortune, OD, PhD**[3], **Balwantray C. Chauhan, Ph.D**[5], **Claude F. Burgoyne, MD**[1]

[1]Devers Eye Institute, Optic Nerve Head Research Laboratory, Legacy Research Institute, Portland, OR, USA

[2]Department of Ophthalmology, Medical College, the Catholic University of Korea, Seoul, Korea

[3]Devers Eye Institute, Discoveries in Sight Research Laboratories, Legacy Research Institute, Portland, OR 97208-3950, USA

[4]Department of Ophthalmology, Second Xiangya Hospital, Central South University, Changsha, Hunan Province, P.R.China.

[5]Ophthalmology and Visual Sciences, Dalhousie University, Halifax, NS, Canada

[6]Jules Stein Eye Institute, David Geffen School of Medicine at UCLA, Los Angeles, CA, USA

[7]Department of Ophthalmology, School of Medicine, University of Alabama at Birmingham, Birmingham, Alabama, United States.

[8]Einhorn Clinical Research Center, Moise and Chella Safra Advanced Ocular Imaging Laboratory, New York Eye and Ear Infirmary of Mount Sinai Health System, New York, USA

[9]Department of Ophthalmology, University of Erlangen, Erlangen, Germany.

[10]Wilmer Eye Institute, Johns Hopkins University, Baltimore, MD, USA

[11]Department of Ophthalmology, University of Heidelberg, Heidelberg, Germany

Abstract

Corresponding Author: Claude F. Burgoyne, Optic Nerve Head Research Laboratory, Devers Eye Institute, Legacy Research Institute 1225 NE 2nd Ave Portland, OR 97208-3950, Tel: +1 503 413 4739, cfburgoyne@deverseye.org. **Address for reprints:** Attn: Claude F. Burgoyne, cfburgoyne@deverseye.org, Optic Nerve Head Research Laboratory, Devers Eye Institute, Legacy Research Institute, 1225 NE 2nd Ave, Portland, OR 97232.

Presented in part at the Association for Research in Vision and Ophthalmology Annual Meeting, May 2018, Honolulu, Hawaii

Purpose: To assess anterior scleral canal opening (ASCO) offset relative to Bruch's membrane opening (BMO) (ASCO/BMO offset) so as to determine neural canal direction, obliqueness, and minimum cross-sectional area (NCMCA) in 362 healthy eyes.

Design: Cross-sectional study

Methods: After OCT optic nerve head (ONH) and retinal nerve fiber layer thickness (RNFLT) imaging, BMO and ASCO were manually segmented. Planes, centroids, size and shape were calculated. Neural canal direction was defined by projecting the neural canal axis vector (connecting BMO and ASCO centroids) onto the BMO plane. Neural canal obliqueness was defined by the angle between the neural canal axis and the BMO plane perpendicular vector. NCMCA was defined by projecting BMO and ASCO points onto a neural canal axis perpendicular plane and measuring the area of overlap. The angular distance between superior and inferior peak RNFLT was measured and correlations between RFNLT, BMO, ASCO, ASCO/BMO offset and NCMCA were assessed.

Results: Mean (SD) NCMCA was significantly smaller than either BMO or ASCO area (1.33 (0.42), 1.82 (0.38), 2.22 (0.43) mm^2, respectively), and most closely correlated to RNFLT ($p<0.001$, $R^2 = 0.158$). Neural canal direction was most commonly superior-nasal (55%). Mean neural canal obliqueness was 39.4° (17.3 °). The angular distance between superior and inferior peak RNFLT correlated to neural canal direction, ($p \leq 0.008$, $R^2 = 0.093$).

Conclusions: ASCO/BMO offset underlies neural canal direction, obliqueness and NCMCA. RNFLT is more strongly correlated to NCMCA than to BMO or ASCO, and its peripapillary distribution is influenced by neural canal direction.

Keywords

Neural Canal; Glaucoma; Optic Nerve Head; 3D Imaging; Optical Coherence Tomography; Imaging Anatomy; Bruch' Membrane Opening; Anterior Scleral Canal Opening

Introduction

The optic disc is the clinical term for the clinically visible surface of the optic nerve head (ONH). Optic disc "size", "shape", "tilt" and "torsion" are common clinical terms that attempt to convey the three-dimensional (3D) complexity of the ONH neural and connective tissue architecture. However, these traditional parameters and their quantification remain two dimensional (2D) whether generated from conventional fundus photographs or from infrared reflectance images produced by modern imaging devices such as optical coherence tomography (OCT).[1–6] While there is a large body of research that uses OCT-detected anatomy to quantify optic disc size, shape, tilt and torsion,[7–14] most studies still rely on an estimate of the clinical disc margin and a host of assumptions to do so.[4–691516]

The underlying anatomy of the disc margin is traditionally defined to be the "scleral lip" or "scleral ring".[17–19] However recent OCT studies[20–23] have shown that the OCT-detected anatomy underlying the clinical disc margin varies among ONH sectors in most human eyes. While the disc margin is commonly defined by BMO, unpigmented Bruch's Membrane, and the Border Tissues of Elschnig, it can also involve unpigmented peripapillary sclera and/or

the anterior scleral canal opening (ASCO).[20–22] Frequently, the innermost extension of Bruch's membrane beyond the border tissues is invisible to the clinician, making disc margin based "disc size" estimates inaccurate.[20–22]

We use the term *"neural canal"* to define the path of the retinal ganglion cell (RGC) axons through the ONH.[24] The neural canal includes *pre-scleral* and *scleral canal* regions (Figure 1) and extends from BMO through the anterior and posterior scleral canal openings. We propose that the size, shape and offset of the ASCO relative to BMO, (ASCO/BMO offset) determine the direction, obliqueness and minimum cross-sectional area of the pre-scleral neural canal. We predict that these components of neural canal architecture contribute to the 2D clinical concepts of optic disc "size", "shape", "tilt" and "torsion" and hypothesize that incorporation of accurate 3D neural canal anatomy into OCT-based glaucoma detection algorithms will eventually improve their sensitivity and specificity.

As a first step towards incorporating 3D OCT characterizations of ONH neural canal architecture into the detection of glaucoma, the purpose of the present study was to quantify the size, shape and offset of the ASCO relative to BMO so as to determine ONH neural canal direction, obliqueness and minimum cross-sectional area (NCMCA) in a large group of healthy eyes. A second purpose of this study was to report and compare the influence of ocular and demographic factors on these parameters and assess their correlation to global and sectoral retinal nerve fiber layer thickness (RNFLT), ONH minimum rim width (MRW) and area (MRA).[25–27] Finally, we set out to lay a conceptual and computational foundation for the incorporation of OCT-detected neural canal anatomy into OCT characterizations of ONH tilt, rotation and peripapillary scleral bowing in future studies.

Methods

Detailed descriptions of our study participants and our methods of data acquisition have been published,[28–30] We use the term ONH to refer to the tissues that are contained within the scleral canal and those immediately adjacent to it (i.e., the peripapillary sclera, choroid and retina as well as the immediate retrolaminar optic nerve).

Participants.

A total of 362 healthy individuals were recruited from 8 centers (5 in the United States, 2 in Germany and 1 in Canada).[28–30] Among these 246 self-identified as European Descent,[30] 47 as Hispanic Ethnicity, 47 as African Descent, 19 as Asian Descent, and 3 as Native American Descent participants. Inclusion criteria included: age 18 to 90 years old; no history of glaucoma, IOP < 21mmHg; best corrected visual acuity > 20/40, refraction less than ±6.00 diopter (D) sphere and ±2.00D cylinder; (4) Glaucoma Hemifield Test and Mean Deviation within normal limits. Exclusion criteria included: unusable stereo photographs or insufficient OCT image quality (quality score<20); clinically abnormal optic disc appearance; any intraocular surgery (except uncomplicated cataract surgery) or vitreous, retinal, choroidal or neurophthalmological disease; and racial or ethnic group other than those listed. All test procedures were performed on both eyes of each participant, but only one eye was randomized for analysis.

Participants were recruited to represent the ethnic composition of the US population[31] as mandated by the US Food and Drug Administration. Each participant provided signed informed content. The study adhered to the declaration of Helsinki for research involving human participants and was approved by the institutional review board of each participating institution.

At the first visit, a medical and ophthalmic history was obtained, followed by anterior segment and external eye examinations, Van Herrick angle assessment, crystalline lens evaluation, standard Snellen or Early Treatment Diabetic Retinopathy Study (ETDRS) visual acuity, refraction, central keratometry, and axial length assessments. Standard automated perimetry [Humphrey Field Analyzer (Carl Zeiss Meditec, Dublin, CA), 24-2 Swedish Interactive Thresholding Algorithm] was repeated once if deemed unreliable or outside normal limits (see below). OCT imaging, ophthalmoscopic examination of the posterior pole, and stereophotography were followed by Goldmann applanation tonometry and pachymetry.

OCT Image Acquisition and Segmentation.

The ONH, peripapillary RNFL and macula were imaged with spectral domain OCT (Spectralis, Heidelberg Engineering GmbH, Heidelberg, Germany, software version Heyex 1.9.10.0). For each eye, prior to image acquisition, refractive correction and keratometry values were entered. The operator then manually identified and marked the fovea in a live B-scan, then centered the imaging field on the ONH, where the 2 BMO points in each of 2 perpendicular ONH radial B-scans were identified. These steps established the eye-specific, fovea-BMO (FoBMO) axis, which was used as the reference for the acquisition of all OCT B-scans.[3233] The complete ONH imaging pattern consisted of 24 radial B-scans (15° apart with each B-scan containing 768 A-scans) centered on BMO and acquired in EDI[34] mode, with an average of 25 repetitions each.

Our strategy for OCT ONH image manual segmentation has been described previously (Figure 1).[2829] Raw OCT volumes were exported from the device and imported into a custom 3D visualization and segmentation software (ATL 3D Suite).[35] ONH and peripapillary landmarks were manually segmented in each radial B-scan and the ONH was reconstructed 3-dimensionally. Segmented landmarks included: the internal limiting membrane (ILM); posterior surface of the RNFL, posterior surface of the Bruch's membrane/retinal pigment epithelium complex, BMO, neural canal wall, anterior scleral surface, and the ASCO (segmented on each side of the canal by visually projecting the plane of the peripapillary anterior scleral surface through the neural canal wall and marking their intersection).[28, 29] All manual segmentations were performed by observers at the Optic Nerve Head Research Laboratory, Devers Eye Institute.

ASCO and BMO Size and Shape.

Quantification of all parameters was performed with Matlab R2016a (Matlab version 9.0.0.341360; The MathWorks, Natick, MA). All left eye data were converted to right eye configuration. A plane was fitted to the 48 segmented BMO and ASCO points, respectively, (Figures 1 and 2), satisfying a least mean square error restraint.[36] The BMO coordinates

were projected to the BMO reference plane. Thereafter, a best-fit ellipse was fitted,[36] and the BMO centroid, area and ovality index, (ellipse long axis / ellipse short axis) were calculated. An ASCO centroid, area, and ovality index were similarly calculated within the ASCO reference plane.

ASCO/BMO Centroid Offset Magnitude and Direction.

ASCO/BMO centroid offset (hereafter ASCO offset) magnitude and direction were defined by projecting the ASCO/BMO centroid vector (the vector connecting the BMO and ASCO centroids) to the BMO reference plane (Figures 2, 3 and 4). ASCO/BMO offset magnitude was defined within the BMO reference plane by the length of the projected ASCO/BMO centroid vector. ASCO/BMO offset direction was defined within the BMO reference plane by the angle between the projected ASCO/BMO centroid vector and the FoBMO axis measured clockwise relative to the FoBMO axis (which was 0°, Figure 2). The superior-inferior and nasal-temporal vectoral components of the projected ASCO/BMO centroid vector were also calculated (Figure 2).

Neural Canal Axis, Direction and Obliqueness.

The neural canal axis was defined by the vector connecting the BMO and ASCO centroids, (Figure 3). Neural canal direction and ASCO/BMO offset direction are therefore identical by definition, the same (Figure 3). Neural canal direction was also measured relative to the FoBMO axis (Figure 3) within the BMO reference plane. Neural canal obliqueness was defined by the angle between the neural canal axis vector and the BMO centroid vector, (a vector perpendicular to the BMO plane that passes through the BMO centroid) (Figure 3).

ASCO/BMO Centroid Depth.

ASCO/BMO centroid depth, (hereafter ASCO/BMO depth) is defined to be the distance of the ASCO centroid from the BMO reference plane measured along a BMO normal vector (Figure 4). It is one estimate of the distance between the ASCO and BMO openings, however the actual distance between these openings will not be constant when ASCO is “tilted” relative to BMO (which is not addressed in this study but will be the subject of a future report).[37]

Neural Canal Minimum Cross-sectional Area (NCMCA).

NCMCA (Figure 5 and supplemental video) estimates the size and shape of the smallest opening through which the RGC axons must pass as they traverse the pre-scleral neural canal. It is a conceptual rather than an anatomically defined opening because it is generated from the projection of surfaces that are not necessarily proximal to one another and because axons are flexible and are not confined to only passing parallel to the canal axis (i.e. they may be able to turn and pass perpendicularly through ASCO and BMO. It was calculated by generating a plane perpendicular to the neural canal axis (the neural canal perpendicular plane), projecting the BMO and ASCO points onto it and quantifying the area that is common to both projections. NCMCA ovality was calculated as outlined for BMO and ASCO, above.

Pre-scleral neural canal volume (NCV).

Pre-scleral NCV, (hereafter NCV), is the volume defined by the BMO plane, ASCO plane and the pre-scleral neural canal boundary (Figure 1, Legend) and was calculated using a convex hull model within Matlab.

MRW, MRA, RNFLT, and the angular distance between the superior and inferior RNFLT peaks.

For each eye, MRW and MRA were calculated from the 24-radial ONH B-scans as previously described.[25] Global and 30° sectoral RNFLT were generated from the standard RNFL circle scan. The angular locations of superior and inferior peak RNFLT were measured relative to the FoBMO axis as depicted in Figure 6.

Inter-observer reproducibility.

Inter-observer segmentation reproducibility was assessed for all parameters within the manual segmentations of 4 independent operators from the same 8 OCT data sets.

Statistical Analysis.

All statistical analyses were performed with IBM SPSS Statistics (version 24.0, International Business Machines (IBM) Corp., Armonk, NY). Intraclass correlation coefficients (ICC) between observers for each parameter were calculated using a two-way mixed model for agreement. The effects of age, axial length, gender, ethnicity, and IOP on all neural canal parameters were assessed using multivariate linear regression.

Results

Three hundred sixty two eyes of 362 participants were studied. Demographic and ocular data for all 362 participants are summarized in Table 1. As Asian and Native American descent subjects were few, ethnicity differences were assessed among European Descent, Hispanic Ethnicity, African Descent, and a combined Asian and Native American Descent group for subsequent analyses. Age, axial length, ASCO area, IOP and CCT were not significantly different by ethnicity ($p \geq 0.060$), nor was the proportion of females and left eyes (χ^2 test, $p \geq 0.410$). Central corneal thickness and spherical equivalent were statistically different among the ethnic groups ($p \leq 0.012$), with the Asian/Native American Descent subjects having the thickest corneas, the African Descent subjects having the thinnest corneas, the Asian/Native American Descent subjects being the most myopic and the European Descent subjects being the least myopic (Table 2).

Inter-observer Reproducibility.

All parameters showed excellent reproducibility (ICC > 0.8), with ICC values ranging from 0.889 to 0.999 (Supplemental Table 1).

BMO, NCMCA and ASCO Size and Shape.

Plots of the size and shape of BMO, NCMCA and ASCO from all 362 study eyes (Figure 7) illustrate the more circular shape of BMO and the ASCO compared to the more elliptical

shape of NCMCA and their relative size differences (ASCO > BMO > NCMCA). The distribution and frequency of BMO area, NCMCA and ASCO area are shown in Figure 8. The mean (standard deviation (SD)) for BMO area, NCMCA and ASCO area were 1.82 (0.38), 1.33 (0.42) and 2.22 (0.43), mm^2, respectively (all significantly different from one another, $p < 0.001$ by Wilcoxon Signed Rank test). The distribution and frequency of individual-eye discordance between NCMCA and BMO area and NCMCA and ASCO area are shown in Figure 8. The mean NCMCA/ASCO ratio (60.4% (16.4)) was significantly smaller than the mean NCMCA/BMO ratio (73.5% (19/1)) ($p < 0.001$ by Wilcoxon Signed Rank test). While BMO and the ASCO were similarly circular, (mean ovality indices 1.120 (0.06) and 1.118 (0.06), respectively, $p = 0.746$ by Wilcoxon Signed Rank test), NCMCA, (mean ovality index 1.538 (0.56), was significantly more elliptical, than both, ($p < 0.001$ by Wilcoxon Signed Rank test).

NCV.

Mean (SD) NCV was 22.91×10^7 (6.58×10^7) μm^3, range (8.63×10^7 to 45.36×10^7 μm^3) (Table 3).

ASCO/BMO Offset and Depth.

The distribution and frequency of ASCO/BMO offset magnitude and direction are shown in Figure 9 with representative cases of extreme ASCO/BMO offset highlighted in each clinical quadrant. Mean ASCO offset magnitude was 89.01 μm (± 63.15). Mean ASCO/BMO offset direction was 145.03° (± 61.3) (i.e. within the superior nasal quadrant), with 60.5% of eyes demonstrating superior nasal ASCO offset relative to BMO, 14.6% inferior nasal offset, 20.2% superior temporal offset and 4.7% inferior temporal offset. Mean (SD) ASCO/BMO depth was 93.01 (24.24) μm, range (33.73 to 160.08 μm) (Table 3).

Neural Canal Direction and Obliqueness.

Neural canal direction, as determined by ASCO/BMO offset direction, (Figure 9), is reported above. Mean neural canal obliqueness, measured relative to the BMO normal vector (0°) and BMO reference plane (90°) was 39.4° (17.3 °), (range 0.8° - 76.2°) (Figure 10), with the most oblique canals occurring in the eyes with the greatest ASCO/BMO offset (Figure 10).

Correlations with RNFLT.

Larger BMO area, NCMCA, ASCO area and NCV correlated with increased global RNFL thickness (Figure 11, $p \leq 0.005$, and $R^2 = 0.038$, 0.158, 0.026 and 0.038, by linear regression, respectively, with the correlation between NCMCA and global RNFLT being significantly stronger than for ASCO are, BMO area and NCV ($p < 0.001$, Steiger's test). Correlations between MRW and each opening were weaker, ranging from $R^2 = 0.034$ to $R^2 = 0.076$. Correlations for MRA were similar to MRW for ASCO and NCMCA, and were predictably higher with BMO, ($R^2 = 0.241$), (since BMO contributes to MRA calculation).[25, 28]

Correlations between ASCO/BMO offset and the location of the superior and inferior RNFLT peaks.

The angular distance between the superior and inferior RNFLT peaks modestly correlated to the nasal-temporal vectoral component of ASCO/BMO offset (Figure 12), $p < 0.001$ and $R^2 = 0.088$) and was not correlated to either the fovea to BMO centroid distance or the fovea to ASCO centroid distance (Supplemental Figure 1). The correlation between the nasal-temporal and superior-inferior components of ASCO/BMO offset direction and sectoral RNFLT are shown in Figure 12. Sectoral RNFLT thickness was more strongly influenced by the nasal-temporal component of ASCO/BMO offset than the superior-inferior component ($p < 0.001$ Steiger's test). Correlations between all twelve 30° sectoral components of ASCO/BMO offset direction and sectoral RNFLT thickness are shown in Supplement Figure 2.

Demographic and ocular effects.

Within a univariate analysis of each factor, (Table 2) and multivariate linear regression analysis, (Supplemental Tables 2 and 3), male gender was associated with an increased superior-inferior component of ASCO/BMO offset magnitude. Increased age was associated with a decrease in BMO area ($p = 0.029$), ASCO area ($p = 0.001$), NCMCA ($p < 0.001$), NCV and ASCO/BMO depth ($p < 0.001$) and an increase in NCMCA ovality ($p = 0.046$) and neural canal obliqueness ($p = 0.023$).

An increase in axial length was associated with a decrease in NCMCA ($p < 0.001$), and an increase in NCMCA ovality ($p < 0.001$), ASCO/BMO offset magnitude ($p < 0.001$) and direction ($p < 0.046$) and neural canal obliqueness ($p < 0.001$). Imaging day IOP was not associated with any parameter. BMO area in the Hispanic Ethnicity and Asian and Native American Descent cohorts was larger than the European and African Descent cohorts ($p \leq 0.002$). NCMCA within the Hispanic Ethnicity and African Descent cohorts was larger than the European and Asian and Native American Descent cohorts ($p \leq 0.001$). NCV was significantly smaller in European Descent eyes compared to all others. European Descent subjects demonstrated larger ASCO/BMO offset magnitude, a larger nasal-temporal component of ASCO/BMO offset than Hispanic and African Descent subjects ($p \leq 0.021$) and a larger ASCO/BMO offset direction angle and greater neural canal obliqueness than Hispanic Descent subjects ($p < 0.018$).

Discussion

This study introduces the use of OCT imaging to clinically quantify the size, shape and offset of the ASCO relative to BMO in healthy human eyes. It then used this anatomy to determine the direction, obliqueness and minimum cross-sectional area of the pre-scleral portion of the ONH neural canal. In so doing, it enables the incorporation of ONH neural canal direction, obliqueness and minimum cross-sectional area into OCT strategies to structurally detect and stage the optic neuropathies of human glaucoma and myopia. It also lays the conceptual and computational foundation for future OCT characterizations of ONH tilt, rotation and peripapilary scleral bowing in glaucomatous and myopic eyes. Finally, in

introducing the parameter NCMCA, (see Supplemental Video), it advances an ongoing discussion regarding the anatomic and biomechanical implications of clinical “disc” size.

Our findings suggest that the NCMCA is smaller and more elliptical than either BMO or ASCO. Furthermore, NCMCA most closely correlated to global and sectoral RNFLT compared to BMO, ASCO area or NCV. Neural canal direction was most commonly superior nasal and the magnitude of the nasal-temporal component of this offset correlated to the sectoral location of the superior and inferior peak RNFLT (i.e., the distribution of RNFLT and to a lesser degree the rim tissue) relative to the FoBMO axis. Neural canal obliqueness was substantial in our study eyes and greatest in eyes in which ASCO/BMO offset was greatest. Finally, racial and ethnic differences, as well as gender differences in all components of NC direction and obliqueness were modest as were the strength of the most important demographic (age) and ocular (axial length) associations.

Several seminal studies have suggested that the amount of rim tissue and/or the number of optic nerve axons correlate to clinical disc margin based “disc size”.[38–40] Using OCT to estimate the smallest portion of the axonal passage way between BMO and ASCO, (the NCMCA), provides a new OCT concept for estimating the normal amount of RGC axon-related neuronal tissue for a given eye. By normal, we mean the largest amount of neuronal tissue that was present at the completion of development, prior to subsequent age-related axon loss. The R^2 value between NCMCA and global RNFLT (0.158), while modest, was 4-fold than that between BMO area and RNFLT (0.038) which is the current OCT standard.[30, 41] Because RNFLT is correlated to axial length in our data, ($p = 0.001$; $R^2 = 0.035$), partial correlations between RNFLT and NCMCA, BMO, and ASCO areas adjusted for axial length were performed and found to be 0.371 ($P<0.001$), 0.193 ($P=0.001$) and 0.175 ($P=0.002$), respectively. These correspond to R^2 values of 0.138, 0.037 and 0.031, respectively. We propose that RNFLT be corrected for NCMCA, age and axial length to derive the most accurate cut-off values for normative data and to potentially improve diagnostic accuracy in glaucoma detection.

The fact that NCMCA more strongly correlated with RNFLT than ASCO, BMO or the volume they define, (NCV), suggests a relationship between this aspect of the neural canal and the amount of neural tissue at the end of development. However, given the deviations from expected retinal ganglion cell axon topography that have been described in the retina,[42] lamina cribrosa,[43] and orbital optic nerve,[44] it is not likely that all axons pass parallel to the neural canal axis within the pre-scleral neural canal. It therefore should not be assumed that NCMCA “limits” the number of axons in a given eye. In a cross-sectional study in which all eyes started with exactly the same RNFLT regardless of NCMCA, the same finding would be present if age-related RGC axon loss was significantly higher in eyes with smaller NCMCA. Of interest, within the multivariable analysis of effects on RNFLT, while the interaction between age and NCMCA achieved significance, ($p \leq 0.041$), the R^2 value was minimal (0.014). Longitudinal studies starting in early childhood will be required to determine if one or both of these mechanisms contribute to the relationship between NCMCA and RNFLT that we describe.

Previous studies have suggested that the sectoral distribution of RNFL thickness can be influenced by a variety of ocular and biometric factors that include the position of the retinal vasculature,[45–49] the position of the temporal raphe relative to the FoBMO axis,[50] the distance from the fovea to the center of the clinical disc margin,[51] the FoBMO angle,[52] axial length,[51, 5354] and the size, shape and "torsion" of the clinical disc margin.[505556] Based on our finding that the nasal-temporal component of ASCO/BMO offset correlated to the sectoral location of the superior and inferior peak RNFLT, our data suggest that components of neural canal direction be incorporated into glaucoma detection strategies that predict the "normal" sectoral distribution of RNFLT, in a given eye.

NCMCA is quantified by projecting BMO and ASCO points onto a plane that is perpendicular to the neural canal axis. Therefore, unlike BMO and ASCO, the NCMCA is not an actual opening, being instead an estimate of the smallest area through which the axons must pass. While the size and shape of the NCMCA may influence axonal susceptibility within the ONH, incorporation of the NCMCA into biomechanical engineering models that predict IOP/CSF related ONH connective tissue loading[57–61] should be undertaken with caution. We predict that neural canal direction and obliqueness contribute to RGC axonal susceptibility within the pre-scleral and scleral (lamina cribrosa) portions of the neural canal. Based on an ONH biomechanics literature that emphasizes the importance of the peripapillary sclera, as well as the size and shape of the scleral canal, to ONH susceptibility,[57–61] we suggest that ASCO size and shape as well as neural canal direction, obliqueness and NCMCA be incorporated into biomechanical models that attempt to predict individual eye susceptibility to glaucomatous damage.[57–61]

Neural canal direction and ASCO/BMO offset direction are both defined by the vector that connects the ASCO and BMO centroids, and are therefore, by definition, the same (Figure 3C). However, in this study we address them individually in part because the phenomenon underlying the term "ASCO/BMO offset" is more clinically intuitive than the term "neural canal direction" and in part because it has been suggested that the relationship between the ASCO and BMO longitudinally changes as part of progressive myopia.[62–64] We suggest "ASCO/BMO offset" be used when talking about processes that primarily affect these structures. We suggest that "neural canal" be used when talking about the RGC axon pathway through the eye wall and/or the amount and susceptibility of its neuronal contents.

Separate from its relationship to neural canal obliqueness and direction, we have previously reported that ASCO/BMO offset identifies the location and extent of oblique border tissue regions and thus directly influences juxta-scleral canal peripapiillary choroidal thickness.[29] We predict that oblique border tissue regions will be most susceptible to longitudinal PCT thinning because PCT is thinnest in these regions. We further predict that longitudinal thinning within oblique border tissue regions will precede the onset and progression of peripapillary microvascular drop out [65–67] and atrophy,[65] in the aging, glaucomatous and myopic eye. Future longitudinal studies should seek correlations between ASCO/BMO offset direction and the onset and progression of peripapillary atrophy.

Age related choroidal thinning can influence the position of BMO relative to the sclera as first described by Johnstone, et al,[68] and confirmed by us in a separate study.[28] It is therefore

important that in the current study, the perpendicular distance between the ASCO and BMO measured relative to their centroids (ASCO/BMO depth) also decreased (modestly) with age, that it strongly correlates to peripapillary choroidal thickness (PCT) immediately adjacent to the scleral canal (Supplemental Figure 3), ($p < 0.001$, $R^2 = 0.683$, 100 μm from the ASCO), and that the strength of the correlation progressively diminishes as distance from the canal increases ($p < 0.001$, $R^2 = 0.298$, 1100 μm from the ASCO) within PCT data from our recent report,[29] (PCT data not included in the present report). Thus, the age effects on ASCO/BMO depth may be the result of the age effects on PCT, or the result of a common mechanism, and both likely contribute to the age effects on NCV.

We have also previously discussed the fact that we found no differences between the European Descent and African Descent groups in either BMO or ASCO area and that we found BMO area to be larger in Asian and Native American descent eyes compared to European Descent, African Descent and Hispanic Ethnicity eyes.[2829] ASCO/BMO offset magnitude as well as its nasal-temporal vectoral component, neural canal obliqueness and NCMCA ovality were all largest in European Descent and Asian and Native American eyes compared to African Descent and Hispanic Ethnicity eyes. Conversely, NCMCA was smallest in the European Descent and Asian and Native American Descent eyes compared to African Descent and Hispanic Ethnicity eyes.

Because NCMCA and neural canal obliqueness have not previously been studied, there is no literature to place these findings in context. Because European Descent subjects dominate our cohort, the importance of these differences need to be evaluated in larger healthy eye cohorts that are more racially and ethnically diverse. Their potential contributions to ONH susceptibility and their ability to predict the location of early glaucomatous damage must be determined in longitudinal studies. The fact that axial length was not significantly associated with BMO and ASCO area, but was negatively associated with NCMCA and positively associated with all other components of ASCO/BMO offset and neural canal obliqueness, suggests that these anatomical features may contribute to our understanding and characterization of the ONH tissues of highly myopic eyes.[6364]

The limitations of this study include the relatively small number of non-European Descent participants which will be addressed by the recent publication of a 258 participant Japanese normative data base,[41] the anticipated completion of the European and Hispanic subgroup expansions to 250 participants each, and the eventual completion of a planned 250 participant normative data base from mainland China. In this paper, (and the papers that precede it),[2829] we identified the ASCO by projecting the immediate peripapillary scleral surface through the border tissues of Elschnig to the neural canal wall boundary, (Figure 1). Unlike BMO, which is an anatomically identifiable structure in most non-myopic[69] eyes by histology and by OCT,[23, 36, 70] the ASCO is not an anatomically identifiable structure in either modality. However, while ASCO was estimated in the described manner, the interoperator reproducibility of ASCO area and all related parameters were excellent in this study.

In myopia, BMO has been shown to shift temporally relative to the ASCO[6264] however which opening is stable and which opening is moving cannot be determined. Our choice of

BMO as the reference landmark for ASCO/BMO offset assessment does not infer that the ASCO has moved relative to BMO nor does it infer that BMO has moved relative to the ASCO. While using either opening as the reference opening has limitations, we chose BMO as the reference landmark for ASCO/BMO offset characterization for the following reasons. First, axons traverse BMO prior to achieving the ASCO, thus, it is more clinically intuitive to characterize ASCO relative to BMO. Second, BMO can be identified in most eyes with OCT,[20367071] whereas OCT visualization of the ASCO is more challenging.[2829] Third, whereas BMO has become a clinically accepted reference landmark for OCT neuroretinal rim measurements ASCO has only recently begun to be identified in OCT images.[2829] Fourth, while BMO size and position may change with age,[28304168] and myopia[6272] our data suggest that ASCO size also decreases with age and previous studies have shown that the ASCO expands and bows outward, in monkey experimental glaucoma.[7374] Thus ASCO may not be more stable than BMO as a reference for our measurements. It may simply be unstable in a different way.

In summary, our study quantifies the size, shape and offset of the ASCO relative to BMO in a large cohort of healthy eyes. We used these data to determine the direction, obliqueness and minimum cross-sectional area of the ONH neural canal. These parameters and concepts may contribute to models that predict the susceptibility of certain eyes to glaucomatous damage and create new indices that may yield higher diagnostic accuracy for the presence and progression of the disease. They also lay the foundation for future OCT characterization of ONH tilt, rotation and peripapilary scleral bowing in eyes that demonstrate the clinical phenomena of optic disc tilt and torsion.

Supplementary Material

Refer to Web version on PubMed Central for supplementary material.

Acknowledgements/Disclosure

a. Funding/Support:

NIH/NEI R01-EY021281; Legacy Good Samaritan Foundation; Heidelberg Engineering, GmbH, Heidelberg, Germany.

b. Financial Disclosure:

SW. Hong: None. H. Yang: None. S. Gardiner: Nonfinancial support – Heidelberg Engineering. H. Luo: None. C. Hardin: None. G. Sharpe: None. J. Caprioli: None. S. Demirel: Financial support - Legacy Good Samaritan Foundation, Carl Zeiss Meditec, Heidelberg Engineering, NIH/NEI R01-EY-019674. C. A. Girkin: Financial support - Heidelberg Engineering. J. M. Liebmann: Financial support - Carl Zeiss Meditec, Topcon, Inc, Alcon Laboratories, Allergan, Inc, Diopsys Corporation, Glaukos Corporation, Heidelberg Engineering, Merz Pharmaceutical, Inc, Optovue, Inc, Quark Pharmaceuticals, Inc, SOLX, Inc. C. Y. Mardin; Financial support - Heidelberg Engineering. H. A. Quigley: Financial support - Heidelberg Engineering. A. F. Scheuerle: Financial support - Heidelberg Engineering. B. Fortune: Financial support - Legacy Good Samaritan Foundation, Inotek Pharmaceuticals. B. C. Chauhan: Financial support - Heidelberg Engineering. C. F. Burgoyne: Financial support - NIH/NEI R01-EY021281, Legacy Good Samaritan Foundation, Heidelberg Engineering.

* The above listed sponsors/funding organizations had no role in the design, conduct, analysis or reporting of this research.

c. Other Acknowledgments

Drs Seungwoo Hong and Hongli Yang contributed equally to this work.

Abbreviations/Acronyms:

ASCO	anterior sclera canal opening
BMO	Bruch's membrane opening
FoBMO	Foveal-BMO
NC	Neural Canal
NCMCA	Neural Canal Minimum Cross-Sectional Area
OCT	optical coherence tomography
ONH	optic nerve head
RNFL	retinal nerve fiber layer
SD	standard deviation

References

1. Vongphanit J, Mitchell P, Wang JJ. Population prevalence of tilted optic disks and the relationship of this sign to refractive error. Am J Ophthalmol 2002;133(5):679–85. [PubMed: 11992866]
2. Tay E, Seah SK, Chan SP, et al. Optic disk ovality as an index of tilt and its relationship to myopia and perimetry. Am J Ophthalmol 2005;139(2):247–52. [PubMed: 15733984]
3. Samarawickrama C, Mitchell P, Tong L, et al. Myopia-related optic disc and retinal changes in adolescent children from singapore. Ophthalmology 2011;118(10):2050–7. [PubMed: 21820741]
4. Park HY, Lee K, Park CK. Optic disc torsion direction predicts the location of glaucomatous damage in normal-tension glaucoma patients with myopia. Ophthalmology 2012;119(9):1844–51. [PubMed: 22595297]
5. Shin HY, Park HY, Park CK. The effect of myopic optic disc tilt on measurement of spectral-domain optical coherence tomography parameters. Br J Ophthalmol 2015;99(1):69–74. [PubMed: 25091955]
6. Park HY, Lee KI, Lee K, et al. Torsion of the optic nerve head is a prominent feature of normal-tension glaucoma. Invest Ophthalmol Vis Sci 2014;56(1):156–63. [PubMed: 25425302]
7. Hwang YH, Yoo C, Kim YY. Characteristics of peripapillary retinal nerve fiber layer thickness in eyes with myopic optic disc tilt and rotation. J Glaucoma 2012;21(6):394–400. [PubMed: 21946540]
8. Hwang YH, Yoo C, Kim YY. Myopic optic disc tilt and the characteristics of peripapillary retinal nerve fiber layer thickness measured by spectral-domain optical coherence tomography. J Glaucoma 2012;21(4):260–5. [PubMed: 21623226]
9. Park HY, Choi SI, Choi JA, et al. Disc Torsion and Vertical Disc Tilt Are Related to Subfoveal Scleral Thickness in Open-Angle Glaucoma Patients With Myopia. Invest Ophthalmol Vis Sci 2015;56(8):4927–35. [PubMed: 26225633]
10. Yamashita T, Sakamoto T, Yoshihara N, et al. Circumpapillary course of retinal pigment epithelium can be fit to sine wave and amplitude of sine wave is significantly correlated with ovality ratio of optic disc. PLoS One 2015;10(4):e0122191. [PubMed: 25848777]
11. Yamashita T, Sakamoto T, Yoshihara N, et al. Correlations between local peripapillary choroidal thickness and axial length, optic disc tilt, and papillo-macular position in young healthy eyes. PLoS One 2017;12(10):e0186453. [PubMed: 29023585]

12. Suh SY, Le A, Shin A, et al. Progressive Deformation of the Optic Nerve Head and Peripapillary Structures by Graded Horizontal Duction. Invest Ophthalmol Vis Sci 2017;58(12):5015–21. [PubMed: 28973373]
13. Shoji T, Kuroda H, Suzuki M, et al. Vertical asymmetry of lamina cribrosa tilt angles using wide bandwidth, femtosecond mode-locked laser OCT; effect of myopia and glaucoma. Graefes Arch Clin Exp Ophthalmol 2017;255(1):197–205. [PubMed: 27796669]
14. Shoji T, Kuroda H, Suzuki M, et al. Correlation between lamina cribrosa tilt angles, myopia and glaucoma using OCT with a wide bandwidth femtosecond mode-locked laser. PLoS One 2014;9(12):e116305. [PubMed: 25551632]
15. Kwun Y, Han G, Choy YJ, et al. Optic Disc Characteristics and Visual Field Progression in Normal Tension Glaucoma Patients With Tilted Optic Discs. J Glaucoma 2016;25(11):901–07. [PubMed: 27755347]
16. Kim YC, Jung Y, Park HL, et al. The Location of the Deepest Point of the Eyeball Determines the Optic Disc Configuration. Sci Rep 2017;7(1):5881. [PubMed: 28725046]
17. Nicolela MT. Optic Nerve: Clinical Examination In: Giaconi JA, Law SK, Coleman AL, et al., eds. Pearls of Glaucoma Management. Berlin, Heidelberg: Springer Berlin Heidelberg 2010:15–21.
18. Fingeret M, Medeiros FA, Susanna R Jr., et al. Five rules to evaluate the optic disc and retinal nerve fiber layer for glaucoma. Optometry 2005;76(11):661–8. [PubMed: 16298320]
19. Cantor LB, Rapuano CJ, Cioffi GA. Chapter 3: Clinical Evaluation. Basic and Clinical Science Course (BCSC) 2017-2018: Glaucoma Section 10. San Francisco, CA: Amer Academy of Ophthalmology 2017-2018:48.
20. Reis AS, Sharpe GP, Yang H, et al. Optic disc margin anatomy in patients with glaucoma and normal controls with spectral domain optical coherence tomography. Ophthalmology 2012;119(4): 738–47. [PubMed: 22222150]
21. Hong SW, Koenigsman H, Ren R, et al. Glaucoma Specialist Optic Disc Margin, Rim Margin, and Rim Width Discordance in Glaucoma and Glaucoma Suspect Eyes. Am J Ophthalmol 2018;192:65–76. [PubMed: 29750947]
22. Hong SW, Koenigsman H, Yang H, et al. Glaucoma Specialist Detection of Optical Coherence Tomography Suspicious Rim Tissue in Glaucoma and Glaucoma Suspect Eyes. Am J Ophthalmol 2018 [published Online First: 2018/11/11]
23. Strouthidis NG, Yang H, Reynaud JF, et al. Comparison of clinical and spectral domain optical coherence tomography optic disc margin anatomy. Invest Ophthalmol Vis Sci 2009;50(10):4709–18. [PubMed: 19443718]
24. Downs JC, Yang H, Girkin C, et al. Three-dimensional histomorphometry of the normal and early glaucomatous monkey optic nerve head: neural canal and subarachnoid space architecture. Invest Ophthalmol Vis Sci 2007;48(7):3195–208. [PubMed: 17591889]
25. Gardiner SK, Ren R, Yang H, et al. A method to estimate the amount of neuroretinal rim tissue in glaucoma: comparison with current methods for measuring rim area. Am J Ophthalmol 2014;157(3):540–9 e1–2. [PubMed: 24239775]
26. Reis AS, O'Leary N, Yang H, et al. Influence of clinically invisible, but optical coherence tomography detected, optic disc margin anatomy on neuroretinal rim evaluation. Invest Ophthalmol Vis Sci 2012;53(4):1852–60. [PubMed: 22410561]
27. Strouthidis NG, Fortune B, Yang H, et al. Longitudinal change detected by spectral domain optical coherence tomography in the optic nerve head and peripapillary retina in experimental glaucoma. Invest Ophthalmol Vis Sci 2011;52(3):1206–19. [PubMed: 21217108]
28. Luo H, Yang H, Gardiner SK, et al. Factors Influencing Central Lamina Cribrosa Depth: A Multicenter Study. Invest Ophthalmol Vis Sci 2018;59(6):2357–70. [PubMed: 29847642]
29. Yang H, Luo H, Gardiner SK, et al. Factors Influencing OCT Peripapillary Choroidal Thickness: A Multi-Center Study. Invest Ophthalmol Vis Sci in press
30. Chauhan BC, Danthurebandara VM, Sharpe GP, et al. Bruch's Membrane Opening Minimum Rim Width and Retinal Nerve Fiber Layer Thickness in a Normal White Population: A Multicenter Study. Ophthalmology 2015;122(9):1786–94. [PubMed: 26198806]
31. Bureau USC. Statistical Abstract of the United States: 2012. In: Commerce USDo, ed. 131 ed: U.S. Census Bureau, 2012:1–940.

32. Burgoyne C The morphological difference between glaucoma and other optic neuropathies. J Neuroophthalmol 2015;35 Suppl 1:S8–S21.
33. Chauhan BC, Burgoyne CF. From clinical examination of the optic disc to clinical assessment of the optic nerve head: a paradigm change. Am J Ophthalmol 2013;156(2):218–27 e2. [PubMed: 23768651]
34. Spaide RF, Koizumi H, Pozzoni MC. Enhanced depth imaging spectral-domain optical coherence tomography. Am J Ophthalmol 2008;146(4):496–500. [PubMed: 18639219]
35. Fortune B, Reynaud J, Hardin C, et al. Experimental Glaucoma Causes Optic Nerve Head Neural Rim Tissue Compression: A Potentially Important Mechanism of Axon Injury. Invest Ophthalmol Vis Sci 2016;57(10):4403–11. [PubMed: 27564522]
36. Strouthidis NG, Yang H, Fortune B, et al. Detection of optic nerve head neural canal opening within histomorphometric and spectral domain optical coherence tomography data sets. Invest Ophthalmol Vis Sci 2009;50(1):214–23. [PubMed: 18689697]
37. Wang YX, Yang H, Luo H, et al. Optical Coherence Tomography (OCT) detected Anterior Scleral Canal Opening (ASCO) Tilt and Rotation relative to Bruch's Membrane Opening (BMO) and Peripapillary Scleral Bowing (PSB) in Healthy Eyes ARVO 2019 Annual Meeting Vancouver, 2019.
38. Caprioli J, Miller JM. Optic disc rim area is related to disc size in normal subjects. Arch Ophthalmol 1987;105(12):1683–5. [PubMed: 3689192]
39. Quigley HA, Brown AE, Morrison JD, et al. The size and shape of the optic disc in normal human eyes. Arch Ophthalmol 1990;108(1):51–7. [PubMed: 2297333]
40. Quigley HA, Coleman AL, Dorman-Pease ME. Larger optic nerve heads have more nerve fibers in normal monkey eyes. Arch Ophthalmol 1991;109(10):1441–3. [PubMed: 1929937]
41. Araie M, Iwase A, Sugiyama K, et al. Determinants and Characteristics of Bruch's Membrane Opening and Bruch's Membrane Opening-Minimum Rim Width in a Normal Japanese Population. Invest Ophthalmol Vis Sci 2017;58(10):4106–13. [PubMed: 28828482]
42. Ogden TE. Nerve fiber layer of the macaque retina: retinotopic organization. Invest Ophthalmol Vis Sci 1983;24(1):85–98. [PubMed: 6826318]
43. Morgan JE, Jeffery G, Foss AJ. Axon deviation in the human lamina cribrosa. Br J Ophthalmol 1998;82(6):680–3. [PubMed: 9797672]
44. Horton JC, Greenwood MM, Hubel DH. Non-retinotopic arrangement of fibres in cat optic nerve. Nature 1979;282(5740):720–2. [PubMed: 514350]
45. Hood DC, Fortune B, Arthur SN, et al. Blood vessel contributions to retinal nerve fiber layer thickness profiles measured with optical coherence tomography. J Glaucoma 2008;17(7):519–28. [PubMed: 18854727]
46. Hood DC, Salant JA, Arthur SN, et al. The location of the inferior and superior temporal blood vessels and interindividual variability of the retinal nerve fiber layer thickness. J Glaucoma 2010;19(3):158–66. [PubMed: 19661824]
47. Pereira I, Weber S, Holzer S, et al. Correlation between retinal vessel density profile and circumpapillary RNFL thickness measured with Fourier-domain optical coherence tomography. Br J Ophthalmol 2014;98(4):538–43. [PubMed: 24390166]
48. Yamashita T, Asaoka R, Tanaka M, et al. Relationship between position of peak retinal nerve fiber layer thickness and retinal arteries on sectoral retinal nerve fiber layer thickness. Invest Ophthalmol Vis Sci 2013;54(8):5481–8. [PubMed: 23847316]
49. Resch H, Pereira I, Weber S, et al. Retinal Blood Vessel Distribution Correlates With the Peripapillary Retinal Nerve Fiber Layer Thickness Profile as Measured With GDx VCC and ECC. J Glaucoma 2015;24(5):389–95. [PubMed: 25719231]
50. Amini N, Nowroozizadeh S, Cirineo N, et al. Influence of the disc-fovea angle on limits of RNFL variability and glaucoma discrimination. Invest Ophthalmol Vis Sci 2014;55(11):7332–42. [PubMed: 25301880]
51. Hong SW, Ahn MD, Kang SH, et al. Analysis of peripapillary retinal nerve fiber distribution in normal young adults. Invest Ophthalmol Vis Sci 2010;51(7):3515–23. [PubMed: 20164448]

52. Choi JA, Kim JS, Park HY, et al. The foveal position relative to the optic disc and the retinal nerve fiber layer thickness profile in myopia. Invest Ophthalmol Vis Sci 2014;55(3):1419–26. [PubMed: 24508789]
53. Zhao JJ, Zhuang WJ, Yang XQ, et al. Peripapillary retinal nerve fiber layer thickness distribution in Chinese with myopia measured by 3D-optical coherence tomography. Int J Ophthalmol 2013;6(5): 626–31. [PubMed: 24195037]
54. Chung HJ, Park CK. Factors determining the peripapillary retinal nerve fiber distribution. J Glaucoma 2014;23(7):471–6. [PubMed: 23970338]
55. Jansonius NM, Schiefer J, Nevalainen J, et al. A mathematical model for describing the retinal nerve fiber bundle trajectories in the human eye: average course, variability, and influence of refraction, optic disc size and optic disc position. Exp Eye Res 2012;105:70–8. [PubMed: 23099334]
56. Lee KH, Kim CY, Kim NR. Variations of retinal nerve fiber layer thickness and ganglion cell-inner plexiform layer thickness according to the torsion direction of optic disc. Invest Ophthalmol Vis Sci 2014;55(2):1048–55. [PubMed: 24458157]
57. Sigal IA, Flanagan JG, Tertinegg I, et al. Modeling individual-specific human optic nerve head biomechanics. Part I: IOP-induced deformations and influence of geometry. Biomech Model Mechanobiol 2009;8(2):85–98. [PubMed: 18309526]
58. Sigal IA, Flanagan JG, Tertinegg I, et al. Modeling individual-specific human optic nerve head biomechanics. Part II: influence of material properties. Biomech Model Mechanobiol 2009;8(2): 99–109. [PubMed: 18301933]
59. Feola AJ, Myers JG, Raykin J, et al. Finite Element Modeling of Factors Influencing Optic Nerve Head Deformation Due to Intracranial Pressure. Invest Ophthalmol Vis Sci 2016;57(4):1901–11. [PubMed: 27088762]
60. Nguyen TD, Ethier CR. Biomechanical assessment in models of glaucomatous optic neuropathy. Exp Eye Res 2015;141:125–38. [PubMed: 26115620]
61. Burgoyne CF, Downs JC, Bellezza AJ, et al. The optic nerve head as a biomechanical structure: a new paradigm for understanding the role of IOP-related stress and strain in the pathophysiology of glaucomatous optic nerve head damage. Prog Retin Eye Res 2005;24(1):39–73. [PubMed: 15555526]
62. Lee KM, Choung HK, Kim M, et al. Positional Change of Optic Nerve Head Vasculature during Axial Elongation as Evidence of Lamina Cribrosa Shifting: Boramae Myopia Cohort Study Report 2. Ophthalmology 2018;125(8):1224–33. [PubMed: 29544962]
63. Kim TW, Kim M, Weinreb RN, et al. Optic disc change with incipient myopia of childhood. Ophthalmology 2012;119(1):21–6 e1–3. [PubMed: 21978594]
64. Kim M, Choung HK, Lee KM, et al. Longitudinal Changes of Optic Nerve Head and Peripapillary Structure during Childhood Myopia Progression on OCT: Boramae Myopia Cohort Study Report 1. Ophthalmology 2018;125(8):1215–23. [PubMed: 29550000]
65. Lee EJ, Lee KM, Lee SH, et al. Parapapillary Choroidal Microvasculature Dropout in Glaucoma: A Comparison between Optical Coherence Tomography Angiography and Indocyanine Green Angiography. Ophthalmology 2017;124(8):1209–17. [PubMed: 28433445]
66. Shin JW, Kwon J, Lee J, et al. Choroidal Microvasculature Dropout is Not Associated With Myopia, But is Associated With Glaucoma. J Glaucoma 2018;27(2):189–96. [PubMed: 29271810]
67. Suh MH, Zangwill LM, Manalastas PI, et al. Deep Retinal Layer Microvasculature Dropout Detected by the Optical Coherence Tomography Angiography in Glaucoma. Ophthalmology 2016;123(12):2509–18. [PubMed: 27769587]
68. Johnstone J, Fazio M, Rojananuangnit K, et al. Variation of the axial location of Bruch's membrane opening with age, choroidal thickness, and race. Invest Ophthalmol Vis Sci 2014;55(3): 2004–9. [PubMed: 24595390]
69. Zheng F, Wu Z, Leung CKS. Detection of Bruch's Membrane Opening in Healthy Individuals and Glaucoma Patients with and without High Myopia. Ophthalmology 2018;125(10):1537–46. [PubMed: 29934269]

70. Strouthidis NG, Grimm J, Williams GA, et al. A comparison of optic nerve head morphology viewed by spectral domain optical coherence tomography and by serial histology. Invest Ophthalmol Vis Sci 2010;51(3):1464–74. [PubMed: 19875649]

71. Strouthidis NG, Yang H, Downs JC, et al. Comparison of clinical and three-dimensional histomorphometric optic disc margin anatomy. Invest Ophthalmol Vis Sci 2009;50(5):2165–74. [PubMed: 19136694]

72. Lee S, Han SX, Young M, et al. Optic nerve head and peripapillary morphometrics in myopic glaucoma. Invest Ophthalmol Vis Sci 2014;55(7):4378–93. [PubMed: 24894400]

73. Yang H, Ren R, Lockwood H, et al. The Connective Tissue Components of Optic Nerve Head Cupping in Monkey Experimental Glaucoma Part 1: Global Change. Invest Ophthalmol Vis Sci 2015;56(13):7661–78. [PubMed: 26641545]

74. Yang H, Downs JC, Girkin C, et al. 3-D histomorphometry of the normal and early glaucomatous monkey optic nerve head: lamina cribrosa and peripapillary scleral position and thickness. Invest Ophthalmol Vis Sci 2007;48(10):4597–607. [PubMed: 17898283]

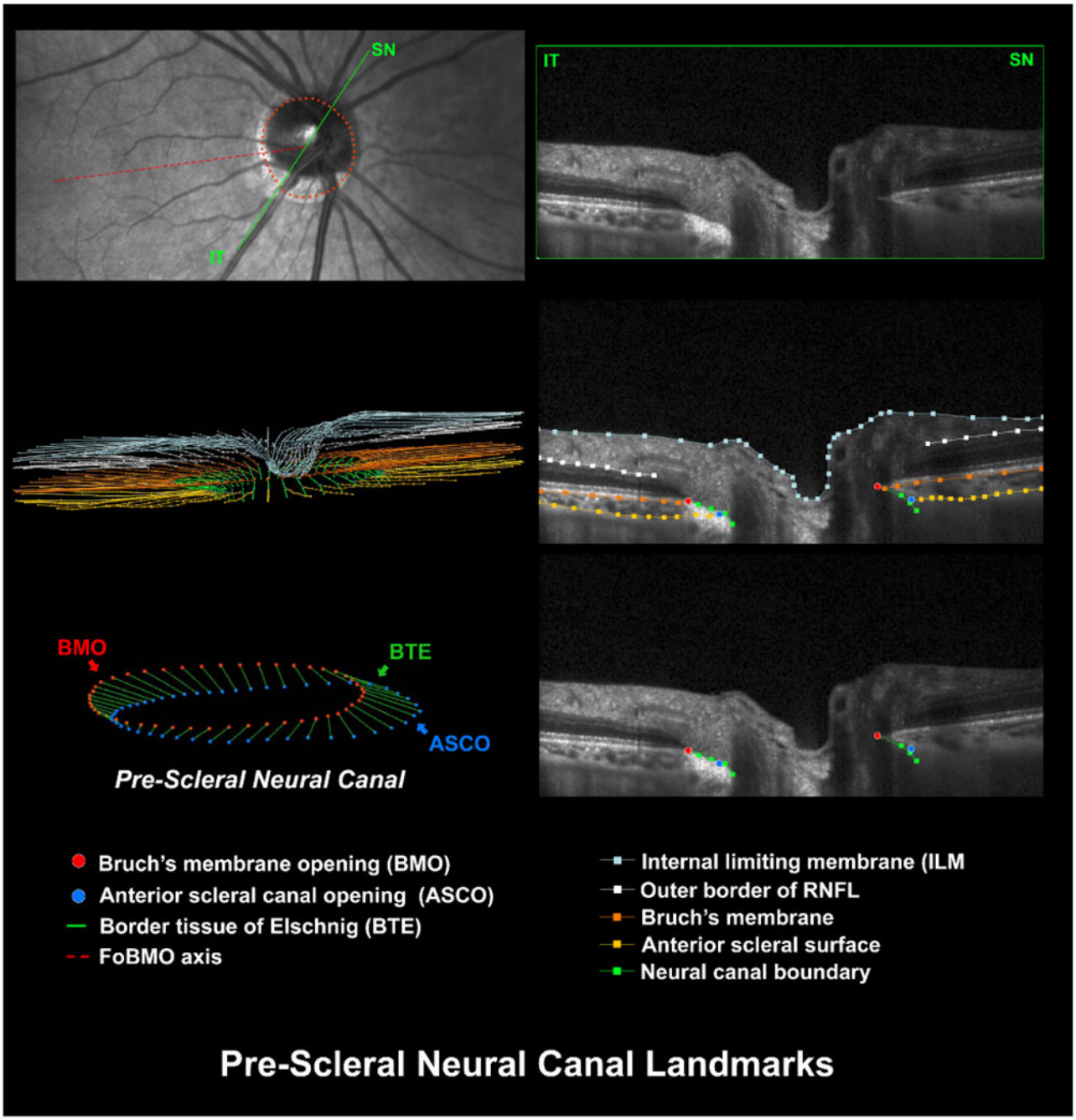

Figure 1. OCT optic nerve head (ONH) and neural canal landmarks from the left eye of study subject FDA 287 shown in right eye orientation.

The ONH neural canal is our term for the axonal pathway through the ONH.[24] It includes pre-scleral and scleral canal regions and extends from Bruch's membrane opening (BMO, red dots in all panels), through the anterior scleral canal opening, (ASCO, blue dots in all panels) and posterior scleral canal openings, (not shown). **(Top Left)** Manually segmented BMO points from a 24-radial B-scan OCT data sets are shown relative to the fovea to BMO centroid (FoBMO) axis (red dotted line). The single green line depicts the representative B-

scan shown in **(Top Right)** (superior-nasal (SN) left and inferior-temporal (IT) right). **(Middle Left)** The 3D point cloud of all segmented OCT ONH landmark points. **(Middle Right)** ONH landmark points segmented within the Top Right panel B-scan. **(Bottom left)** The 48 BMO and ASCO points along with the neural canal boundary points (the Border Tissues of Elshnig (BTE)). Note that the parameter Pre-scleral Neural Canal Volume (NCV), is defined to beh the volume defined by the BMO plane, ASCO plane and the pre-scleral neural canal boundary (BTE) (see methods). **(Bottom Right)** The neural canal landmark points alone segmented within the Top Right panel B-scan. Data from this eye are depicted in right orientation in Figures 1 – 5, and are depicted in their native left eye orientation in Figure 6. Please see our Supplemental Video for a 3D presentation of this anatomy and these concepts.

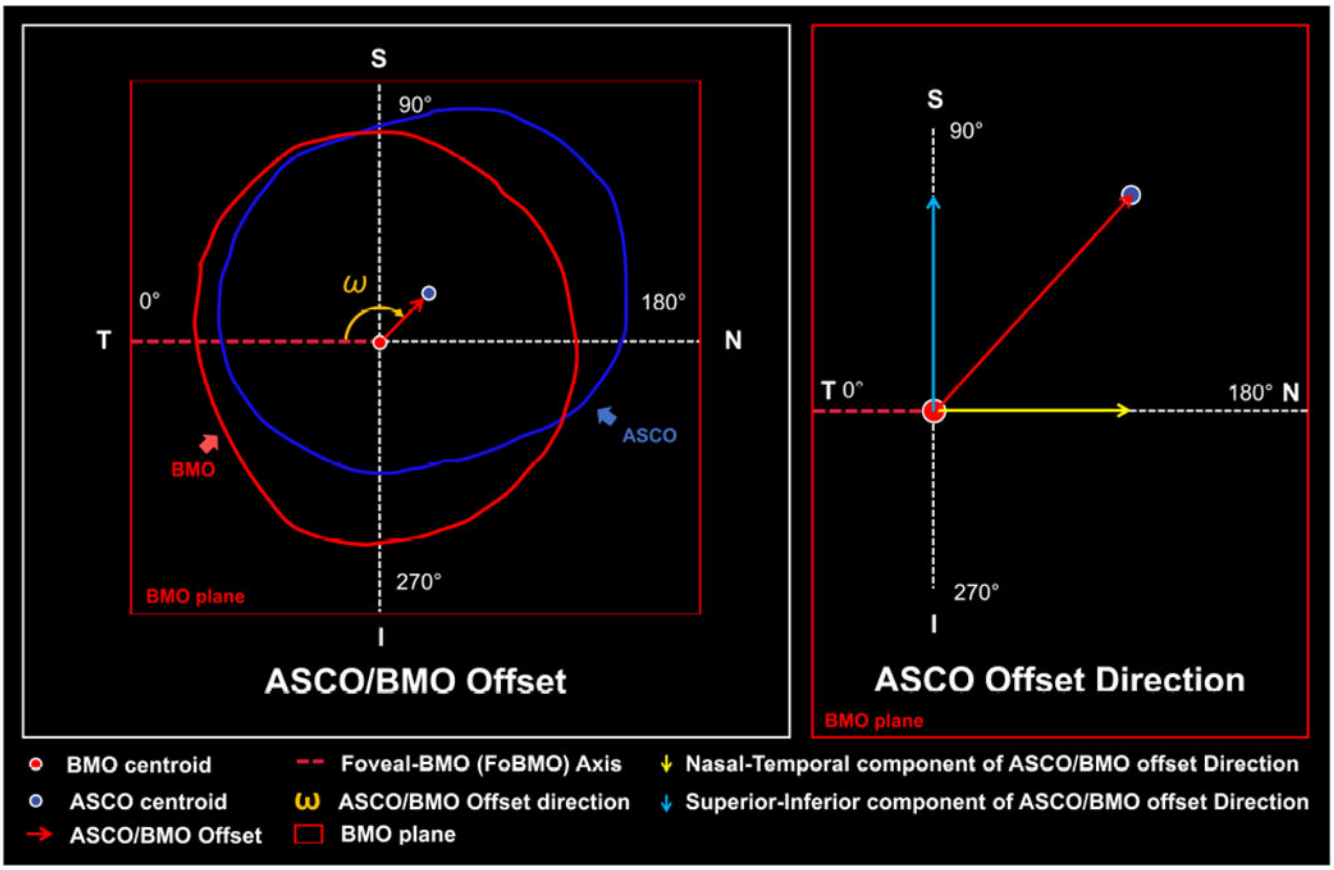

Figure 2. Anterior scleral canal opening (ASCO) offset magnitude and direction relative to Bruch's membrane opening (BMO) are depicted for the eye in Figure 1.

(Left) ASCO/BMO offset is defined by the vector connecting the BMO and ASCO centroids after all ASCO and BMO points are projected to the BMO reference plane. ASCO/BMO offset magnitude is the length of the projected vector within BMO reference plane. By convention, ASCO/BMO offset direction is calculated within the BMO reference plane relative to the Fovea-BMO (FoBMO) axis (0° - temporal, 90° superior, 180° nasal, 270° inferior). It is identical to the parameter "neural canal direction", **(ɯ)** which is explained in Figure 3. **(Right)** Magnified view of (A) which depicts the temporal-nasal (yellow) and superior-inferior (blue) directional component vectors of ASCO/BMO Offset Direction.

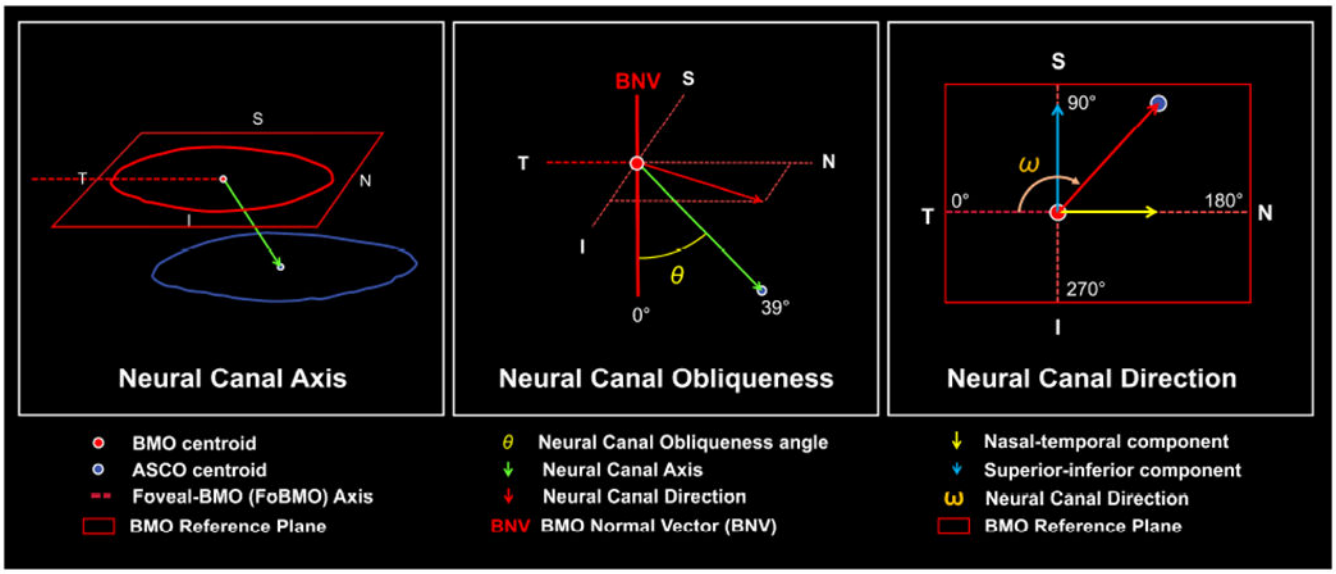

Figure 3. Neural Canal Axis, Obliqueness and Direction are depicted for the eye in Figure 1.

The neural canal is the cellular and connective tissue passage way through the posterior tissues of the eye through which the retinal ganglion cell axons must pass to achieve the orbital optic nerve. It begins at Bruch's membrane opening **(BMO)**, continues through the Border Tissues of Elschnig the anterior scleral canal opening **(ASCO)b** the sclera canal and ends at the posterior scleral canal opening, (not shown). **(Left)** The pre-scleral neural canal is defined by the position of the ASCO relative to BMO. The pre-scleral neural canal axis, (hereafter "neural canal axis"), is defined within 3D space by the vector between the BMO and ASCO centroids, (in green). **(Middle)** Neural canal obliqueness is defined by the angle of the neural canal axis relative to the BMO reference plane normal vector, (hereafter BMO normal vector, **(BNV))** (0° directly perpendicular, 90° parallel to the plane of BMO, 39° in this example). **(Right)** Neural canal direction **(ɯ)** is determined by ASCO/BMO offset direction (Figure 2), and by convention is defined within the BMO reference plane in the same manner. It is the projection of the neural canal axis vector onto the BMO reference plane and is measured relative to the fovea-BMO (FoBMO) axis (0° - temporal, 90° superior, 180° nasal, 270° inferior). Neural canal direction has a nasal-temporal component (yellow) and a superior-inferior component (blue). All data are reported in right eye orientation.

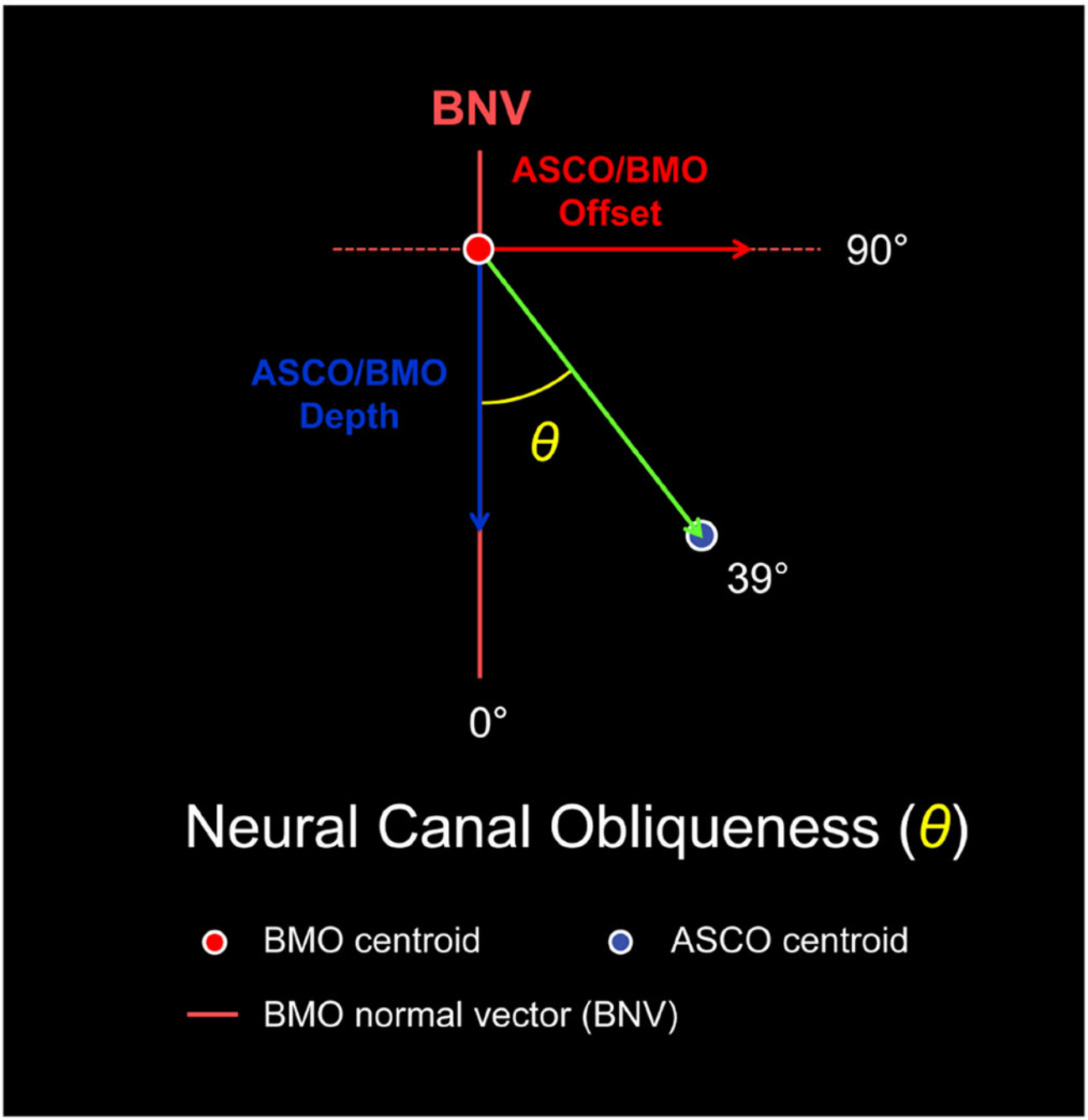

Figure 4. The relationship between the neural canal axis vector, neural canal obliqueness, ASCO/BMO offset and ASCO/BMO centroid depth (hereafter ASCO/BMO depth) as plotted within the neural canal axis plane (the plane that contains all three vectors and all 3 measurements) for the eye in Figure 1.

Within an individual eye the relationship between ASCO/BMO offset and ASCO/BMO depth determines neural canal obliqueness which is measured relative to the BMO normal vector, **(BNV)** (Figure 3). However, within populations of eyes, the relationships between ASCO/BMO offset, depth and neural canal obliqueness are more fluid since many combinations of ASCO/BMO offset and depth can give the same neural canal obliqueness if

the ratio between the two stays constant and many combinations of ASCO offset and depth are possible in any given human eye. ASCO/BMO depth is a measure of the perpendicular distance between the BMO and ASCO centroids. It is one estimate of the distance between the ASCO and BMO openings, however the distance between these openings will not be constant when ASCO is “tilted” relative to BMO (which is not addressed in this report).

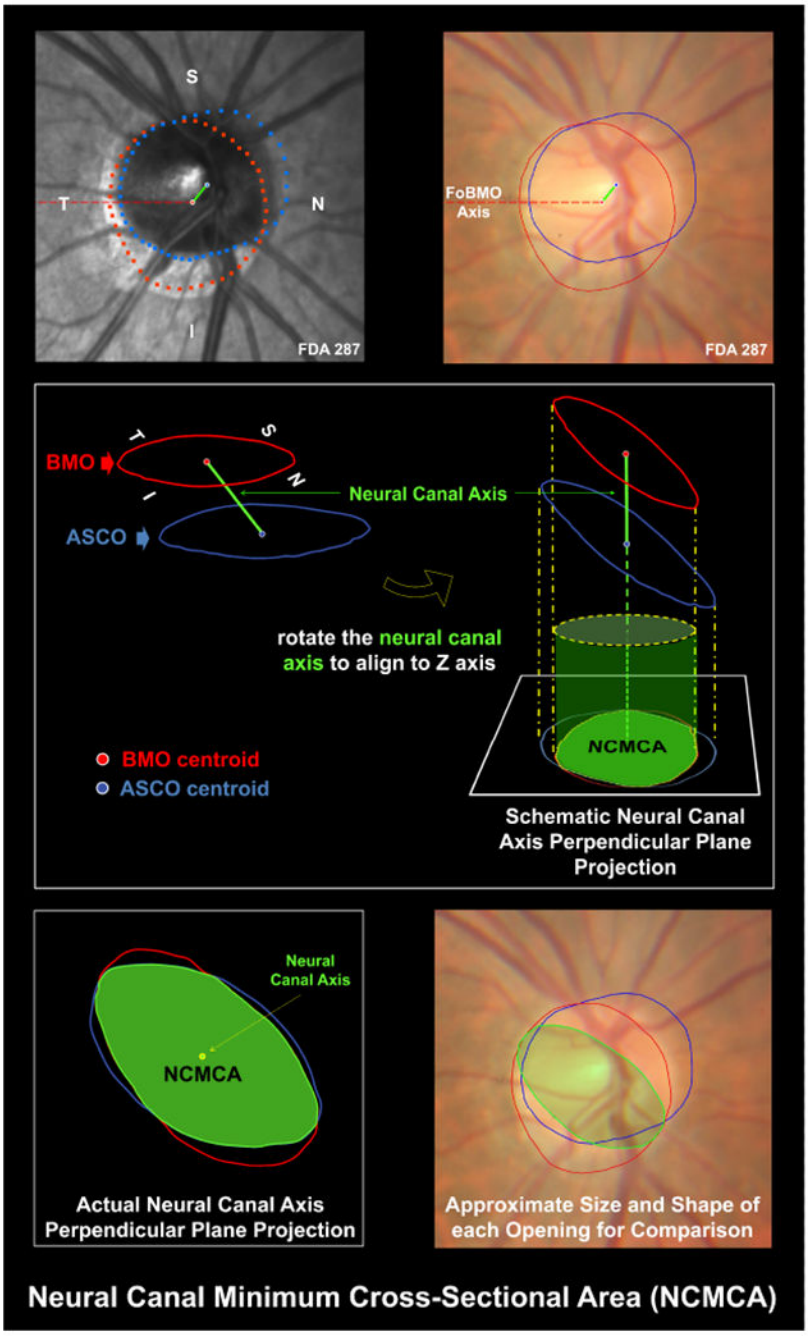

Figure 5. Neural canal minimum cross-sectional area (NCMCA) is calculated within a plane that is perpendicular to the neural canal axis (the neural canal perpendicular plane) for the eye depicted in Figure 1.

(Top Left Panel) Segmented BMO (red) and ASCO (blue) points along with their centroids and the neural canal axis (green) that connects them are shown relative to the Fovea to BMO centroid (FoBMO) axis on the infrared image obtained at the time of OCT imaging. Note that the eye has been rotated so that the FoBMO axis is horizontal to the image frame compared with Figure 1. **(Top Right Panel)** Same structures (BMO and ASCO are now B-spline fitted curves after projection of each point to its respective reference plane), projected

onto a colocalized clinical photograph. **(Middle Panel)** The NCMCA estimates the smallest opening through which the RGC axons pass as they leave the eye. It is calculated by generating a neural canal perpendicular plane (Top right), projecting the BMO and ASCO points onto it and quantifying the area that is common to both projections (bright green, lower right middle panel). **(Lower Left Panel)** The relative size and shape of BMO, ASCO and the NCMCA as projected to the Neural Canal Axis Perpindicular plane are shown, (the neural canal axis is now depicted as a dot because the visualization or projection plane is within the paper this figure is printed on and the axis is perpendicular to it), **(Lower Right Panel)** The actual sizes of each opening are plotted within the BMO reference plane, (rather than projected to it) for comparison purposes. The position of BMO is accurate, but the positions of ASCO and NCMCA are approximated so as to maintain an accurate depiction of their size and shape. Please see our Supplemental Video for a 3D presentation of this anatomy and these concepts.

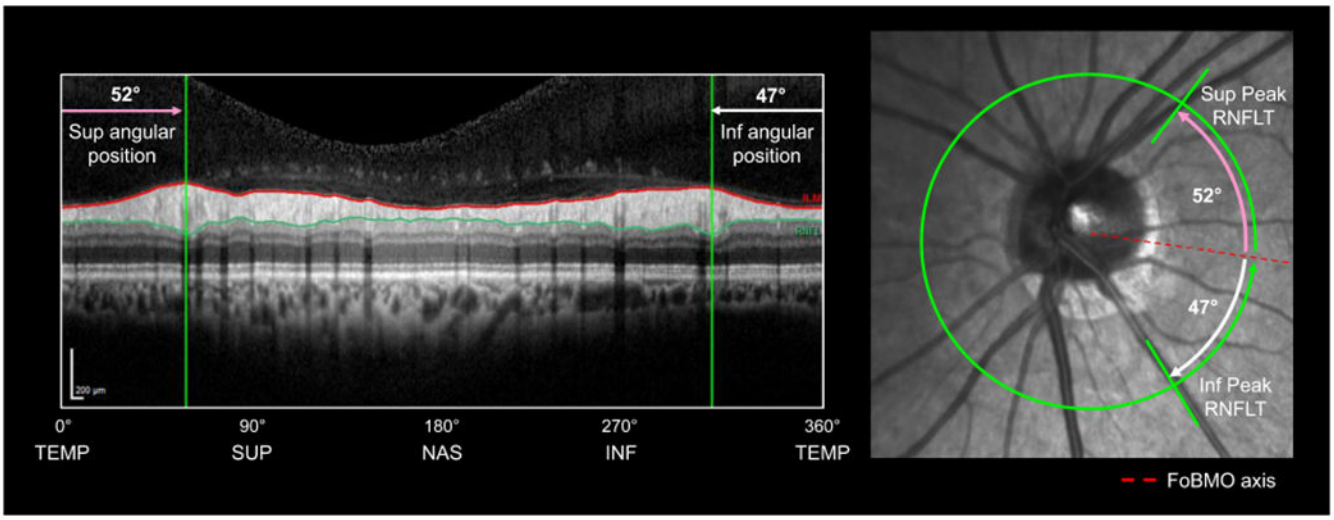

Figure 6. Measurement of the angular distance between the superior and inferior retinal nerve fiber layer thickness (RNFLT) peaks and their superior versus inferior angular asymmetry relative to the fovea-Bruch's membrane opening (BMO) (FoBMO) axis.

(Left) Standard RNFL circle scan with the superior (left) and inferior (right) thickness peaks marked by vertical green lines. **(Right)** The angular distance between the peaks, (marked by radial green segments) is 96° and the two peaks are rotated 5° superiorly relative to the FoBMO axis, (the superior peak being 52° (in pink) and the inferior peak being 47° , (in white)). Measurements are shown for a representative left eye, but all left eye data was converted to right eye orientation for experiment-wide analyses. Images are from the same eye as Figures 1 – 5, but remain in their native, (left eye), orientation.

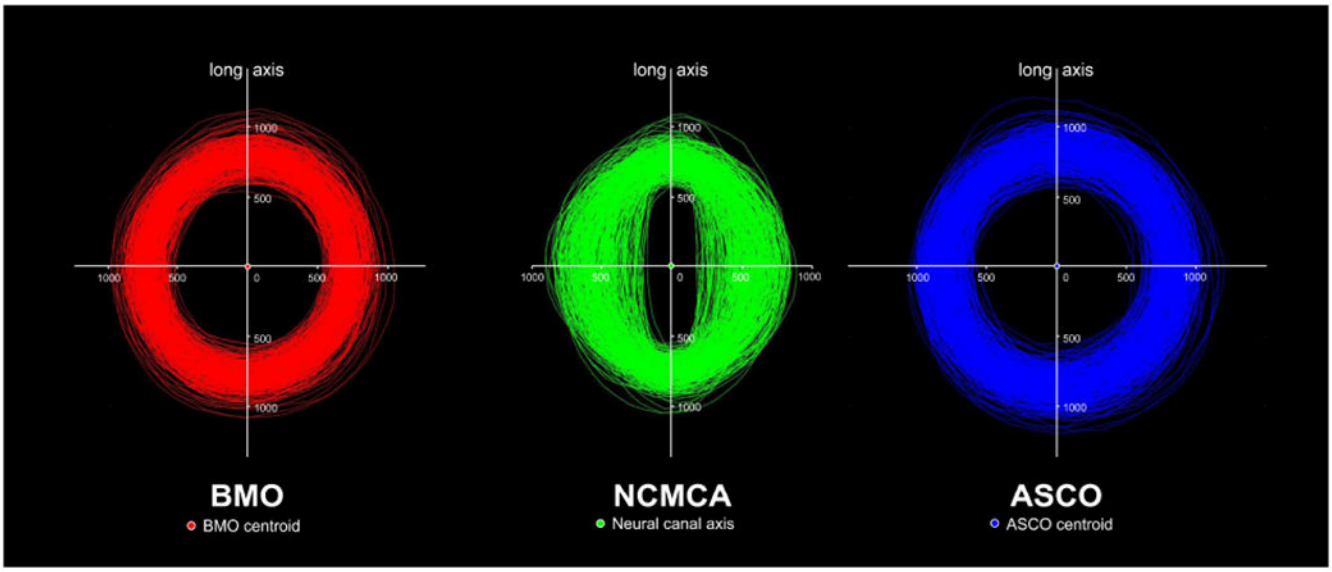

Figure 7. Plots of Bruch's membrane opening, (BMO), (left), the neural canal minimum cross-sectional area (NCMCA), (middle), and the anterior scleral canal opening, (ASCO), (right) from each study eye in the order (left to right) in which they are experienced by the retinal ganglion cell (RGC) axons as they pass through the neural canal.

For each opening type, (BMO, NCMCA and the ASCO), the opening from each eye is plotted such that its centroid is located at the origin and its long axis lies on the vertical axis. Common scaling allows the distribution of size and shape for each opening and between openings to be compared. Note that while all data is in right eye orientation, by using the long axis to orient each subject's opening, there is no consistent anatomic orientation (i.e. the top is not the FoBMO superior). Note that the distribution of the study eye NCMCAs includes a more extensive range of elliptical shapes.

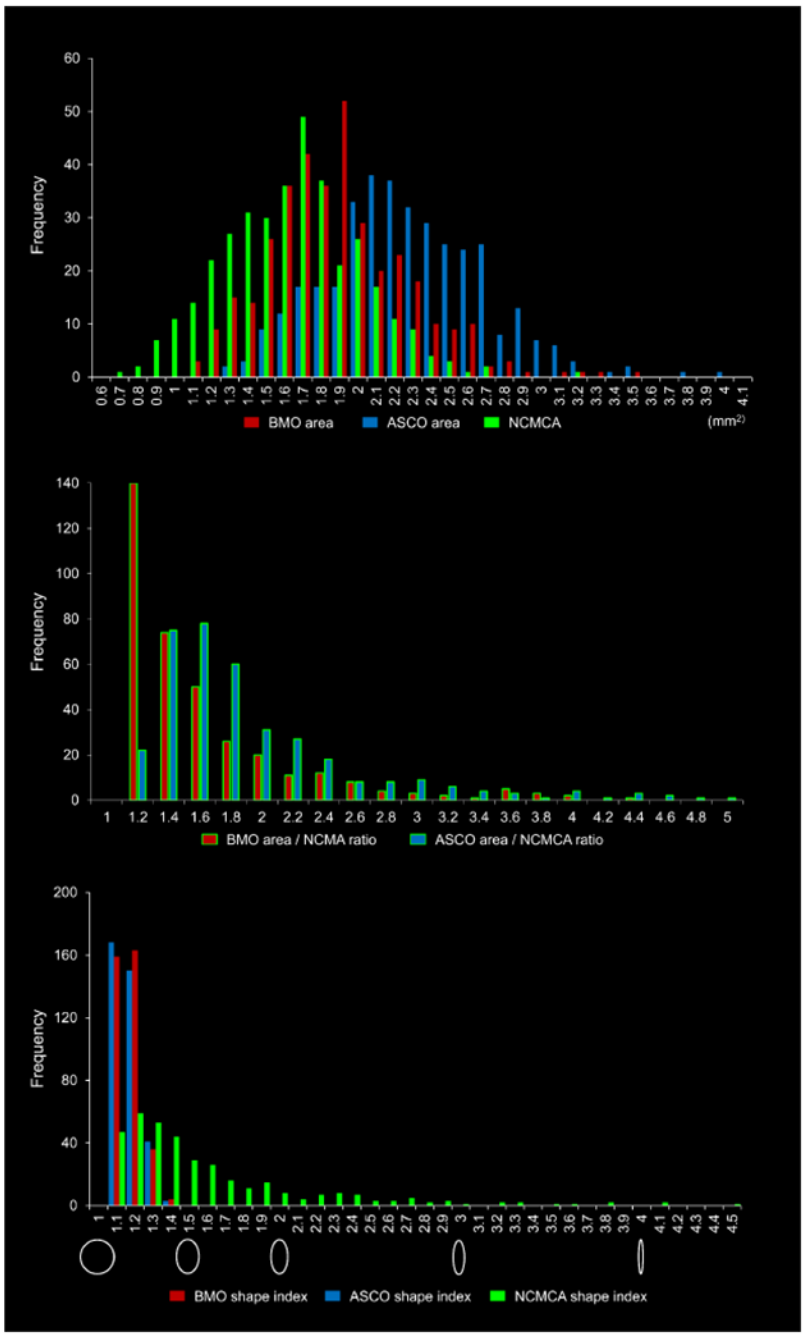

Figure 8. The size distribution, relative size distribution and shape (ovality) distribution of the principal neural canal openings: BMO - Bruch's membrane opening; NCMCA - neural canal minimum cross-sectional area; and the ASCO - anterior scleral canal opening;

(Top) Distribution of BMO area, NCMCA and ASCO area. **(Middle)** Distribution of the ratio between NCMCA and BMO area and the distribution of the ratio between NCMA and ASCO area. **(Bottom)** BMO, NCMCA, and ASCO ovality index (ellipse long axis / ellipse short axis) among all study eyes. Ovality indices of 1.0 (circle), 1.5, 2.0, 3.0 and 4.0 are schematically depicted below the bottom panel.

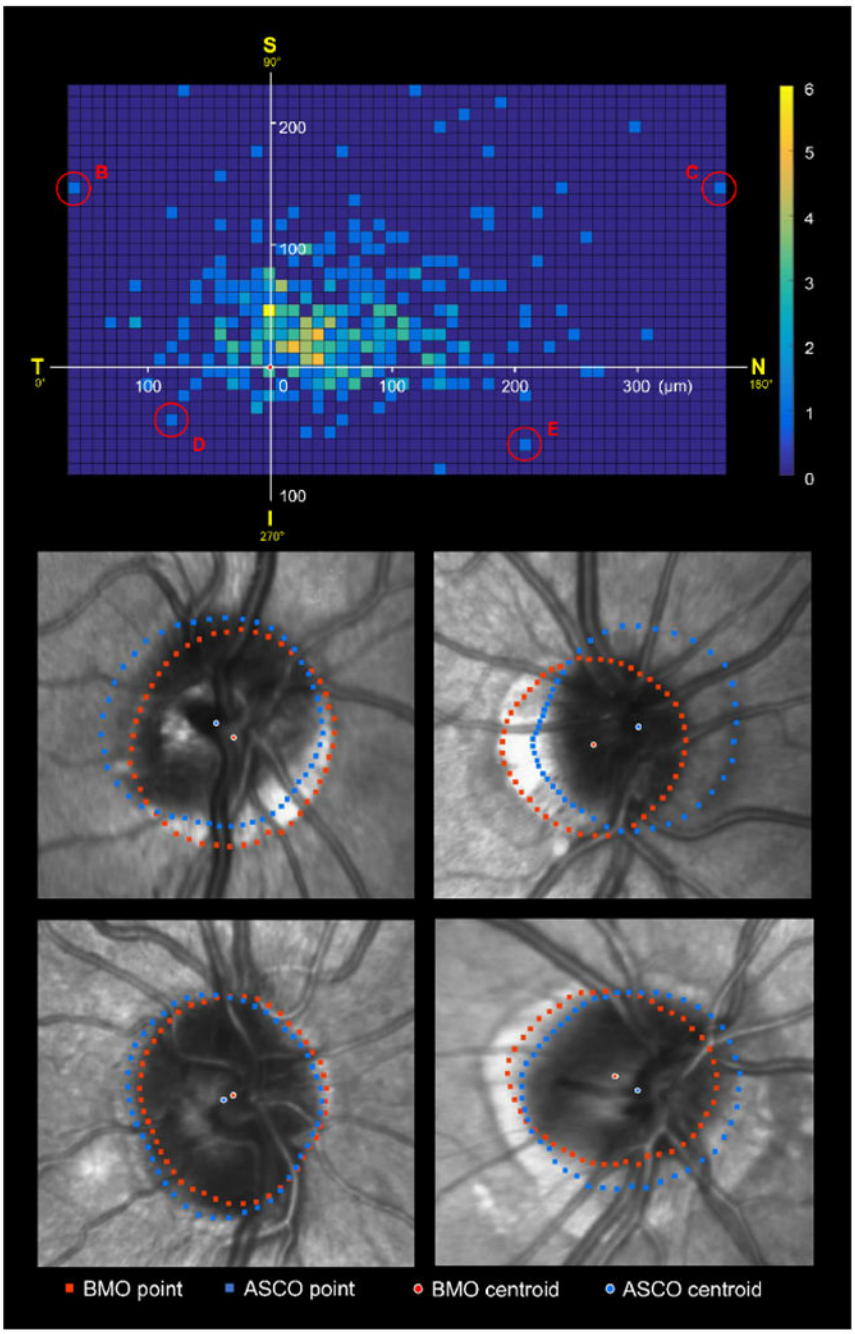

Figure 9. Distribution and Frequency of anterior scleral canal opening (ASCO) vs. Bruch's membrane opening (BMO) offset magnitude and direction among all study eyes.

(Top panel). 2D plot of the position of the ASCO centroid relative to the BMO centroid for all study eyes with the number of eyes at each location denoted by color. The BMO centroid of each eye is located at the origin (0, 0). All data are in right eye orientation. By convention ASCO/BMO offset direction is (0°) when it is directly temporal **(T)**, (90°) when superior **(S)**, (180°) when nasal **(N)** and (270°) when inferior **(I). (Middle to bottom rows)** Representative eyes (marked in red in the top panel, above) from the extreme locations in

each quadrant, (red dots - BMO points, central red dot with white border – BMO centroid; blue dots – ASCO points, central blue dot with white border – ASCO centroid). Note that the parameter neural canal direction also characterizes the angular direction of ASCO/BMO offset, (see Figures 2 and 3), being derived from the same landmarks. Please see our Supplemental Video for a 3D presentation of this anatomy and these concepts.

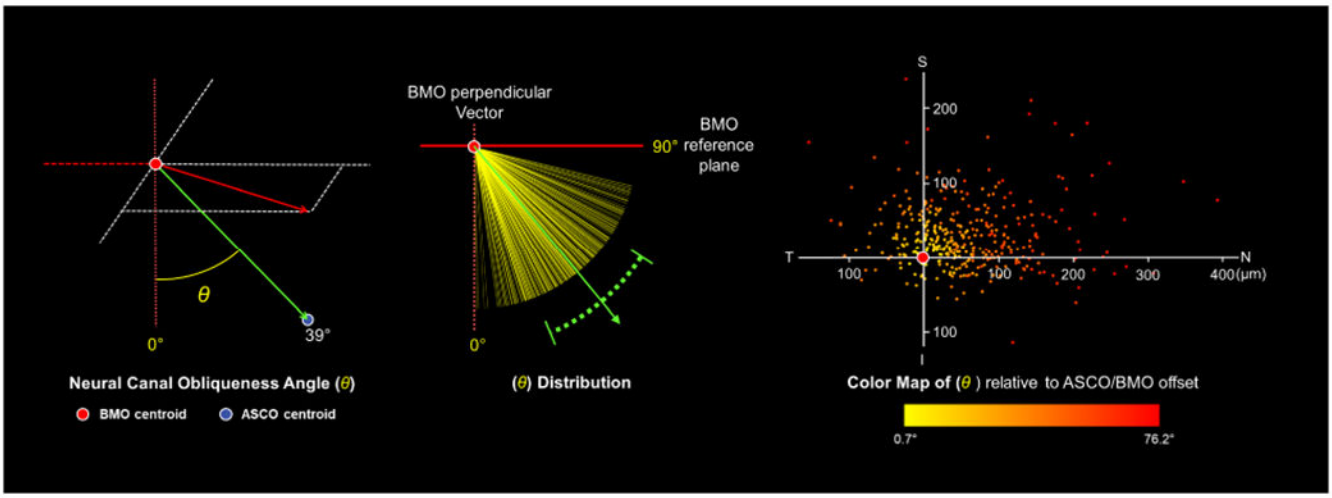

Figure 10. The distribution and frequency of neural canal obliqueness among all study eyes and the relationship between its magnitude and ASCO/BMO offset.

(Left) schematic depiction of neural canal obliqueness angle. **(Middle)** Distribution of neural canal obliqueness among all study eyes relative to the BMO Plane Perpendicular Vector (0°) and the BMO reference plane (90°). The mean neural canal obliqueness angle and the standard deviation of the distribution (39.4° (17.3°)) are depicted in green. The frequency is depicted by the density of the yellow color. **(Right)** As expected, neural canal obliqueness is strongly correlated to ASCO/BMO offset being greatest (red colored dots) in the eyes that are most offset and least (yellow colored dots) in the eyes that are least offset.

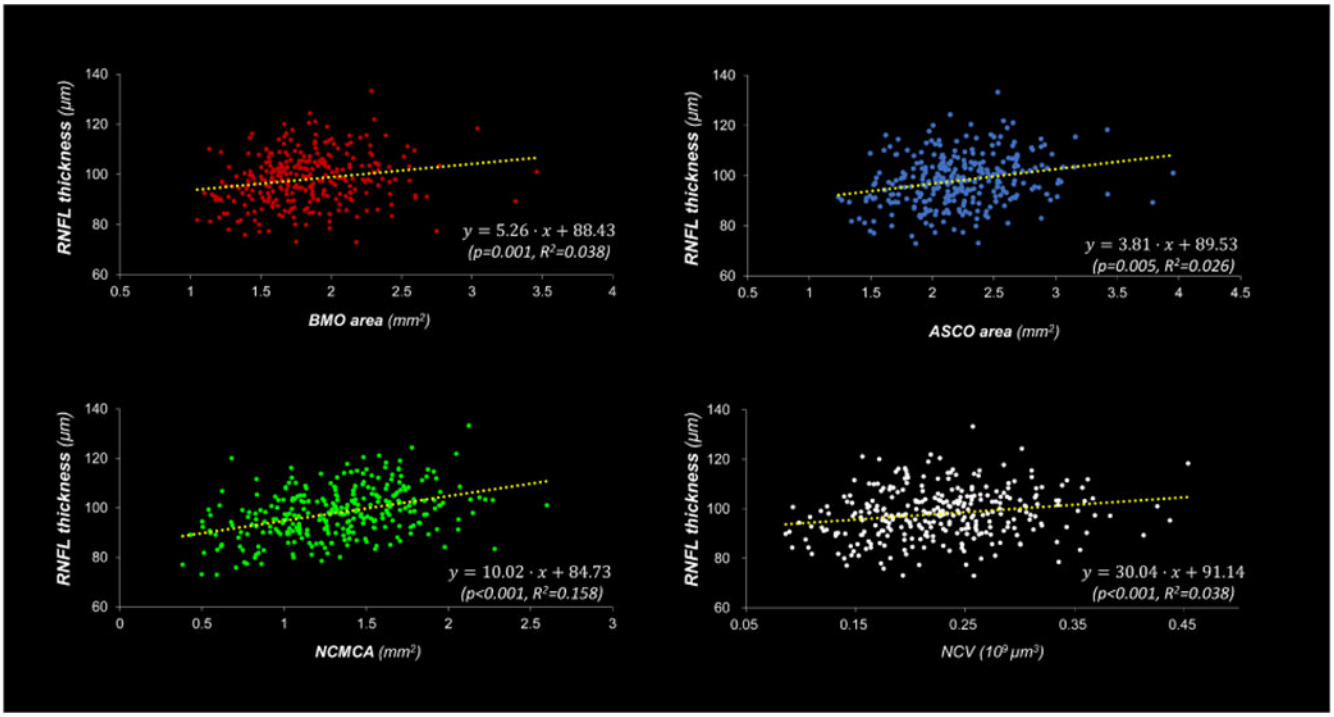

Figure 11. The correlation between global retinal nerve fiber layer thickness (RNFLT) and Bruch's Membrane Opening (BMO) area, anterior scleral canal opening (ASCO) area, neural canal minimum cross-sectional area (NCMCA) and pre-scleral neural canal volume (NCV) is strongest for NCMCA.

Scatterplots of global RNFLT versus BMO area (Top left), ASCO area, (Top right) NCMCA (Bottom left) and NCV (Bottom right). The correlation with global RNFLT was stronger for NCMCA, than for BMO area, ASCO area and NCV ($P < 0.001$, Steiger's test).

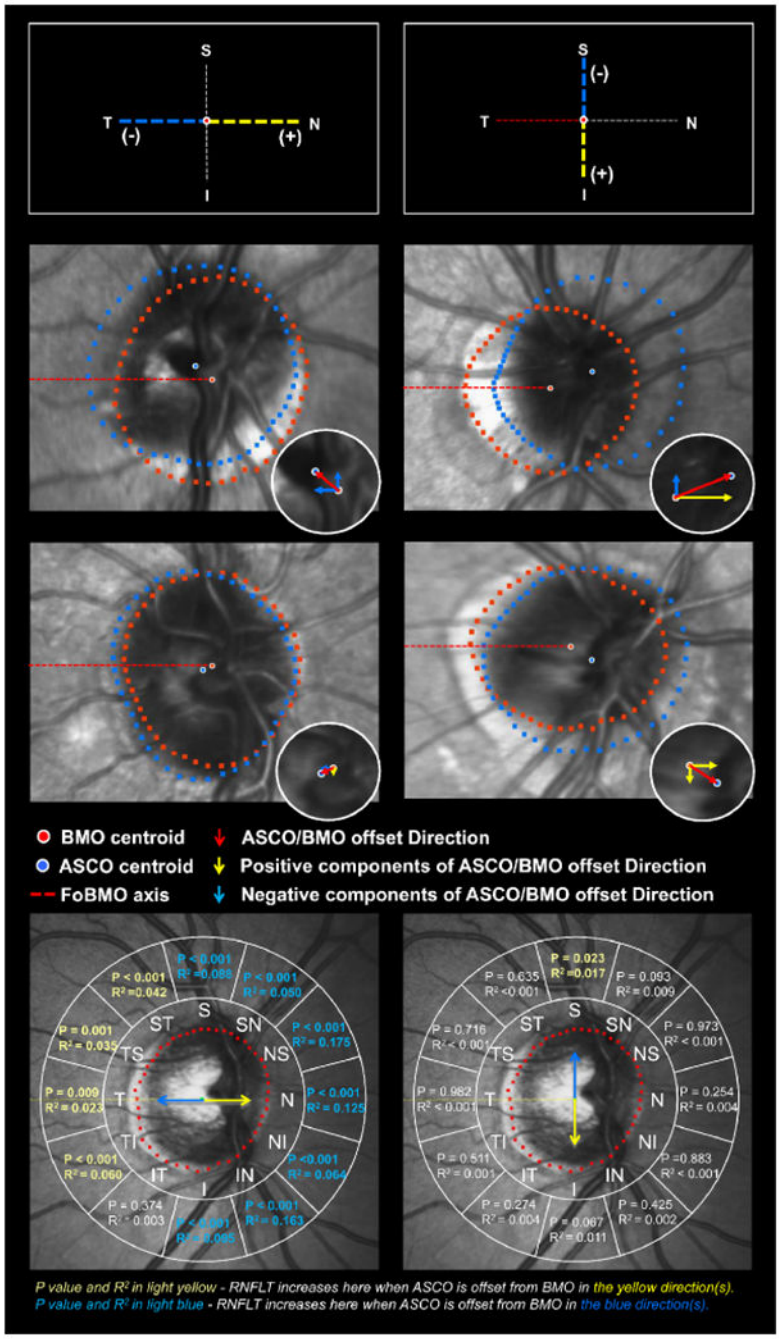

Figure 12. Correlation between the nasal-temporal and superior-inferior components of ASCO/BMO offset direction and sectoral RNFL thickness (RNFLT) among all study eyes.

(Top panels) Sign conventions for the nasal-temporal (Top right) and superior-inferior components (Top left) of ASCO/BMO offset (yellow directions are positive, blue directions are negative). **(Middle two rows)** Representative cases, (from Figure 8), demonstrating ASCO/BMO offset direction in each of the four principal quadrants, (inferior-temporal, (2nd row left); superior-nasal, (2nd row right); inferior-temporal, (3rd row left); and inferior nasal, (2nd row right)). The white circles in each panel depict the ASCO/BMO offset vector for

each eye along with its positive (yellow) or negative (blue) nasal-temporal and superior-inferior components. **(Bottom left)** The correlation between the nasal-temporal component of ASCO/BMO offset and RNFL thickness by sector among all study eyes. These data strongly suggest that when ASCO is “nasal” to BMO, RNFLT decreases in the nasal sectors and increases in the temporal sectors, with the strongest effect occurring in the NS sector, ($p<0.001$, $R^2=0.152$). **(Bottom right)** The correlation between the superior-inferior component of ASCO/BMO offset and RNFL thickness by sector among all study eyes. These data suggest that when ASCO is “inferior” to BMO, RNFLT modestly increases in the S ($p<0.001$, $R^2=0.044$), SN ($p<0.021$, $R^2=0.016$), and NS ($p<0.019$, $R^2=0.016$). These relationships are schematically depicted in Figure 13. **(S)** *superior*, **(SN)** *superior-nasal*; **(NS)** *nasal-superior*, **(N)** *nasal*; **(NI)** *nasal-inferior*, **(IN)** *inferior-nasal*; **(I)** *inferior*, **(IT)** *inferior-temporal*; **(TI)** *temporal-inferior*, **(T)** *temporal*; **(TS)** *temporal-superior*, **(ST)** *superior-temporal.* (See Supplemental Figure 1 for an expanded version of this analysis that addresses the sectoral effects of ASCO/BMO offset on RNFLT for all components of ASCO/BMO offset direction).

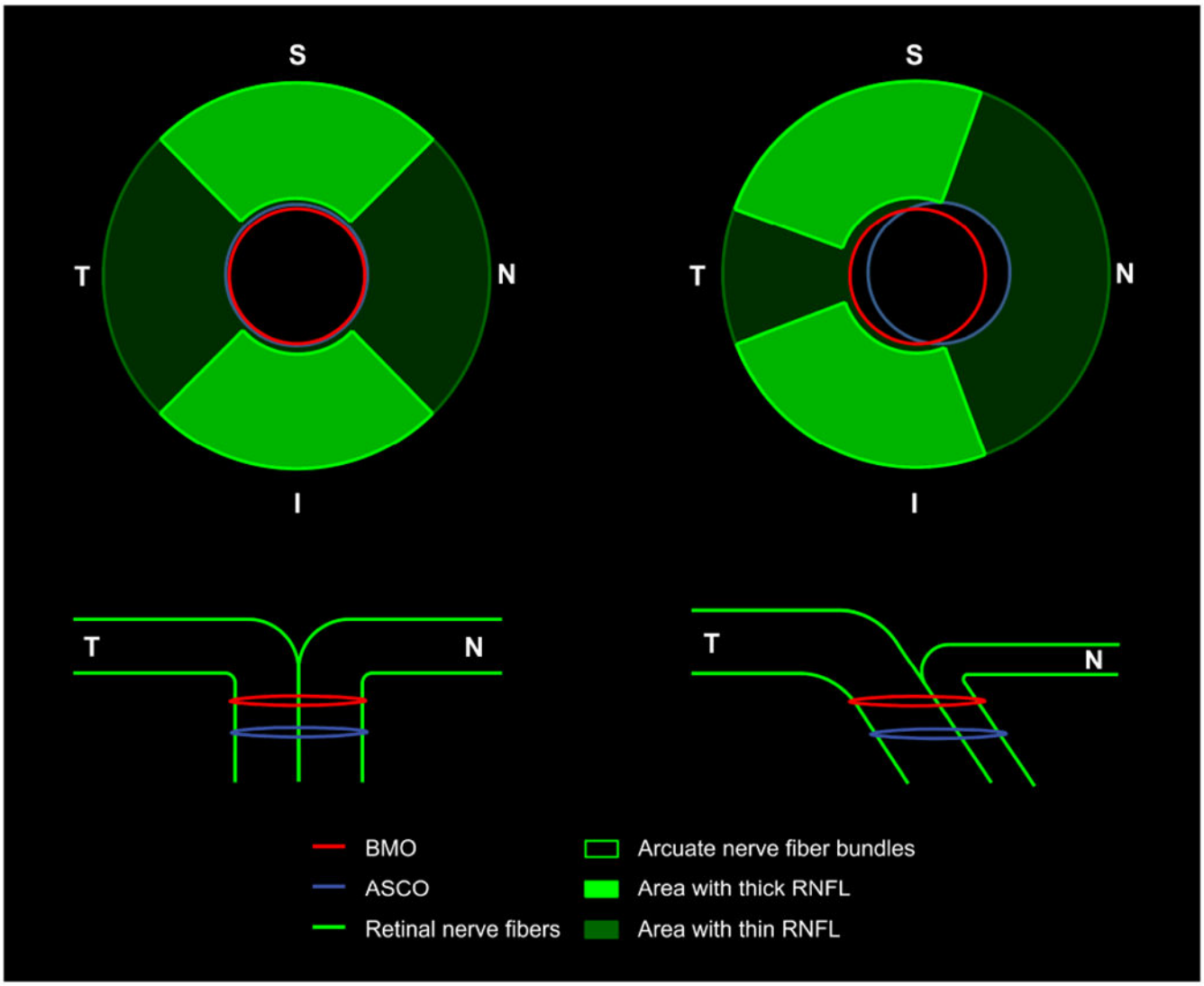

Figure 13. Schematic depiction of the relationship between the nasal-temporal component of ASCO/BMO offset and nasal versus temporal retinal nerve fiber layer (RNFL) thickness.

(Left column). Fundus view (Top left) and cross-sectional view (Bottom left) of an optic nerve head (ONH) with minimal nasal-temporal ASCO/BMO offset. **(Right column)** Fundus view (Top right) and cross-sectional view (Bottom right) of an ONH with considerable nasal-temporal ASCO/BMO offset. Note that the fundus view of the ONH in the top left panel depicts both nasal-temporal ASCO/BMO offset and the shifted location of the superior and inferior arcuate nerve fiber bundles towards the FoBMO axis, (see Figures 5 and 11). Note also that in the bottom right panel the temporal RNFLT is increased and the nasal RNFLT is decreased in compared to the bottom left panel. While the shift of the arcuate bundles in the bottom left panel would be expected to diminish both the superior nasal and inferior nasal RNFLT, our data suggests that the effect is greatest within the superior nasal sectors (see Figure 12).

Table 1.

Demographic and ocular characteristics of the study participants.

	All Subjects (n=362)	European Descent (n=248)	Hispanic Descent (n=47)	African Descent (n=47)	Asian/Native American Descent[1] (n=22)	ANOVA or Chi-Square test (p value)[2]
Female Gender (n (%))	202 (56%)	137 (56%)	30 (64%)	22 (47%)	13 (59%)	0.41[3]
Left Eye (n (%))	181 (50%)	123 (50%)	24 (51%)	25 (53%)	9 (41%)	0.83[3]
Age (year (SD))	50.6 (17.5)	52.2 (18.3)	45.3 (14.1)	49.4 (14.8)	47.3 (19.3)	0.06
Axial Length (mm (SD))	23.7 (0.96)	23.7 (0.91)	23.9 (1.02)	23.8 (1.03)	24.1 (1.11)	0.18
IOP (mmHg (SD))	15 (3)	14.6 (2.7)	14.3 (2.7)	14.9 (2.73)	14 (2.54)	0.49
CCT (μm (SD))	555 (33)	555 (34.5)	556 (26.0)	546 (29.1)	573 (22)	0.012
Spherical Equivalent (diopter (SD))	−0.47 (1.82)	−0.29 (1.72)	−0.43 (1.90)	−0.78 (1.77)	−1.93 (2.14)	< 0.001

IOP (intraocular pressure); CCT (central corneal thickness); SD (standard deviation); ANOVA (analysis of variance) Data are mean (SD)

[1] n=19 (5.2%) Asian and n=3 (0.8%) Native American

[2] ANOVA or Chi-square test to check if ethnicity is significant different for a demographic parameter

[3] Chi-square test

Table 2.

Univariate analysis of the demographic, ocular, ethnicity, gender, and age effects on each Neural Canal parameter.

The number in each cell is the p value of the analysis.

	Gender[1]	Age[2]	Axial Length[2]	IOP[2]	Race/Ethnicity[3]
BMO area (mm^2)	0.511	**0.020**	0.264	0.998	**<0.001**
ASCO area (mm^2)	0.234	**0.001**	0.243	0.525	0.381
NCMCA area (mm^2)	0.647	**0.007**	**<0.001**	0.521	**<0.001**
Neural Canal Volume (μm^3)	0.477	**<0.001**	0.918	0.558	**0.024**
BMO ovality index	0.178	0.740	0.808	0.311	**0.001**
ASCO ovality index	0.053	0.507	0.404	0.462	0.173
NCMCA ovality index	0.976	0.611	**<0.001**	0.716	**0.003**
ASCO/BMO offset magnitude (μm)	0.516	0.073	**<0.001**	0.208	**0.004**
ASCO/BMO offset direction (°)	0.408	0.206	**0.025**	0.205	0.240
Nasal-Temporal ASCO/BMO offset magnitude (μm)	0.159	0.284	**<0.001**	0.204	**0.014**
Superior-Inferior ASCO/BMO Offset Magnitude (μm)	**0.018**	0.094	0.876	0.919	0.593
Neural Canal Obliqueness (°)	0.901	0.126	**<0.001**	0.239	**0.035**
ASCO/BMO Depth (μm)	0.098	**<0.001**	0.705	0.849	0.272

BMO – Bruch's Membrane opening; **ASCO** – Anterior Scleral Canal Opening; **NCMCA** - Neural Canal Minimum Cross-Sectional Area; **IOP** - intraocular pressure; **CCT** - central corneal thickness; **SD** - standard deviation; **ANOVA** (analysis of variance)

[1] t test

[2] Pearson's correlation

[3] ANOVA

Table 3.

Neural canal characteristics of the study participants overall and by racial/ethnic group.

The value in each cell is the mean ± standard deviation and (range).

	All Subjects (n=362)	European Descent (n=248)	Hispanic Ethnicity (n=47)	African Descent (n=47)	Asian and Native American Descent[1] (n=22)
BMO area (mm^2)	1.82 ± 0.38 (1.04 to 3.45)	1.77 ± 0.38 (1.04 to 3.23)	**2.00 ± 0.37** [5] (1.27 to 3.70)	1.80 ± 0.36 (1.13 to 2.76)	**2.03 ± 0.34** [5] (1.10 to 2.52)
ASCO area[6] (mm^2)	2.22 ± 0.43 (1.24 to 3.95)	2.20 ± 0.44 (1.26 to 3.95)	2.30 ± 0.45 (1.47 to 3.07)	2.19 ± 0.41 (1.24 to 3.15)	2.30 ± 0.38 (1.66 to 3.19)
NCMCA area (mm^2)	1.33 ± 0.42 (0.38 to 2.60)	1.27 ± 0.41 (0.38 to 2.60)	**1.54 ± 0.38** [5] (0.68 to 2.28)	**1.47 ± 0.37** [5] (0.51 to 2.32)	1.28 ± 0.48 (0.63 to 2.06)
Neural Canal Volume ($10^7 \mu m^3$)	22.91 ± 6.59 (8.63 to 45.36)	22.18 ± 6.65 (8.63 to 45.36)	**24.53 ± 6.66** [5] **(11.01 to 43.44)**	**24.51 ± 5.76** [5] **(11.92 to 38.23)**	**24.15 ± 6.42 (12.10 to 36.20)**
BMO ovality index	1.12 ± 0.64 (1.00 to 1.36)	1.12 ± 0.06 (1.00 to 1.35)	1.11 ± 0.06 (1.02 to 1.22)	**1.15 ± 0.07** [5] (1.03 to 1.36)	1.11 ± 0.06 (1.03 to 1.25)
ASCO ovality[6] index	1.12 ± 0.64 (1.00 to 1.35)	1.12 ± 0.06 (1.00 to 1.35)	1.10 ± 0.06 (1.02 to 1.24)	1.13 ± 0.07 (1.00 to 1.35)	1.12 ± 0.06 (1.02 to 1.22)
NCMCA ovality index	1.54 ± 0.56 (1.02 to 4.41)	**1.58 ± 0.59** [5] (1.02 to 4.41)	1.39 ± 0.39 (1.02 to 2.67)	1.36 ± 0.31 (1.02 to 2.68)	**1.78 ± 0.78** [5] (1.03 to 4.04)
ASCO/BMO offset magnitude (μm)	89.01 ± 63.15 (1.97 to 401.59)	**92.93 ± 65.19** (1.97 to 401.59)	77.95 ± 53.17 (8.12 to 239.62)	65.90 ± 43.05 (14.60 to 240.73)	**118.15 ± 65.19** [5] (20.67 to 284.17)
ASCO/BMO offset direction[3,6] (°)	145.02 ± 61.31 (1.19 to 358.18)	149.21 ± 55.12 (1.85 to 346.55)	138.83 ± 73.98 (1.19 to 347.69)	137.87 ± 80.50 (6.94 to 358.18)	126.79 ± 47.18 (11.65 to 187.42)
Nasal-Temporal ASCO/BMO offset magnitude (μm)	55.94 ± 76.17 (−153.40 to 393.95)	**64.80 ± 76.46** [5] (−153.40 to 393.95)	34.67 ± 69.36 [5] (−105.59 to 219.42)	38.95 ± 81.18 (−123.68 to 271.98)	**38.67 ± 60.59** (−96.13 to 156.16)
Superior-Inferior ASCO/BMO Offset[6] Magnitude (μm)	30.74 ± 45.21 (−113.44 to 239.62)	29.50 ± 44.55 (−113.44 to 211.10)	31.16 ± 42.84 (−22.59 to 180.57)	30.87 ± 48.17 (−47.58 to 239.62)	43.38 ± 51.88 (−20.35 to 192.83)
Neural Canal Obliqueness[4] (°)	39.36 ± 17.25 (0.77 to 76.22)	**40.82 ± 17.05** [5] (0.77 to 76.22)	34.80 ± 17.38 (3.46 to 73.79)	32.20 ± 13.81 (11.44 to 71.93)	**48.17 ± 19.37** [5] (11.05 to 75.34)
ASCO/BMO Depth (μm)	93.01 ± 24.24 (33.73 to 160.08)	92.19 ± 24.87 (33.73 to 156.33)	99.35 ± 26.32 (60.58 to 160.08)	90.78 ± 19.70 (53.03 to 138.73)	93.58 ± 20.10 (63.46 to 126.44)

BMO – Bruch's Membrane opening; **ASCO** – Anterior Scleral Canal Opening; **NCMCA** – Neural Canal Minimum Cross-Sectional Area;

[1] n=19 (5.2%) Asian and n=3 (0.8%) Native American

[2] ANOVA test to assess if race or ethnicity effects are significant for a given parameter

[3] Also the Neural Canal Direction - measured clockwise from the FoBMO axis (i.e. temporal is 0°)

[4] measured relative to the BMO centroid perpendicular vector

[5] significantly higher than all non-bold groups, but not significantly different from the other bold group if present

[6] Race/Ethnicity was not significant for this parameter by Analysis of Variance, **(ANOVA)**, see Table 2